Molecular Pharmacology Fast Forward. Published on May 30, 2012 as doi: 10.1124/mol.112.078352
This article has not been copyedited and formatted. The final version may differ from this version.

CARBONYLATION INDUCES HETEROGENEITY IN CARDIAC RYANODINE RECEPTORS (RyR2) FUNCTION DURING DIABETES

Chun Hong Shao, Chengju Tian, Shouqiang Ouyang, Caronda J. Moore, Fadhel Alomar, Ina Nemet, Alicia D'Souza, Ryoji Nagai, Shelby Kutty, George J. Rozanski, Sasanka Ramanadham, Jaipaul Singh and Keshore R. Bidasee

From the Departments of Pharmacology and Experimental Neuroscience, Cellular and Integrative Physiology, and Environmental, Occupational and Agricultural Health, University of Nebraska Medical Center, Omaha, NE 68198 (C.H.S., C.T., S.O., C.J.M., F.A., G.J.R., K.R.B.); Department of Pharmacology, University of Dammam, Kingdom of Saudi Arabia (F.A.); Laboratory for Carbohydrate, Peptide and Glycopeptide Research, Rudjer Boskovic Institute, Zagreb, Croatia (I.N.); School of Forensic and Investigative Science, University of Central Lancashire, Preston, UK (A.D., J.S.)**;** Department of Bioscience, School of Agriculture, Laboratory of Food and Regulation Biology, Tokai University, Tokyo, Japan (R.N.); Joint Division of Pediatric Cardiology, University of Nebraska/Creighton University and Children's Hospital and Medical Center, Omaha, Nebraska (S.K.); Nebraska Center for Redox Biology, N146 Beadle Center, Lincoln NE 68588-0662 (K.R.B.); and Department of Physiology and Biophysics, University of Alabama, Birmingham AL, 35244 (S.R.).

Molecular Pharmacology Fast Forward. Published on May 30, 2012 as DOI: 10.1124/mol.112.078352
This article has not been copyedited and formatted. The final version may differ from this version.

Running Title: Carbonylation induces heterogeneity in RyR2 function.

To whom correspondence should be addressed:

Keshore R. Bidasee, Ph.D.

Department of Pharmacology and Experimental Neuroscience,

985800 Nebraska Medical Center, Durham Research Center,

DRC 3047, Omaha, NE 68198-5800

Tel: (402) 559-9018

Fax: (402) 559-7495

E-mail: kbidasee@unmc.edu

Number of text pages – **31**

Number of Tables - **1**

Number of Figures -**10**

Number of References – **62**

Number of words in Abstract -**250**

Number of words in Introduction- **714**

Number of words in Discussion - **1637**

Abbreviations:

RyR2- type 2 ryanodine receptor; **RCS**-reactive carbonyl species; **MGO**-methylglyoxal; **CICR** - Ca^{2+}-induced Ca^{2+}-release; **SERCA2**-sarco(endo)plasmic reticulum Ca^{2+} ATPase; **NCX**-sodium-calcium exchanger; **Glo-1** -glyoxalase-1; **Py**- pyridoxamine; **Ag**- aminoguanidine; **C**-control; **D**- diabetic; **Ins-D**- insulin-treated diabetic; **Py-C**, pyridoxamine-treated control; **Py-D**-pyridoxamine-treated diabetic; **Ag-C**- aminoguanidine-treated control; **Ag-D**- aminoguanidine-treated diabetic; **JSRV**- junctional sarcoplasmic reticulum vesicles.

Molecular Pharmacology Fast Forward. Published on May 30, 2012 as DOI: 10.1124/mol.112.078352
This article has not been copyedited and formatted. The final version may differ from this version.

ABSTRACT

Heart failure and arrhythmias occur at rates 3-5 times higher in individuals with diabetes mellitus compared with age-matched, healthy individuals. Studies attribute these defects in part to alterations in function of cardiac ryanodine receptors (RyR2), the principal Ca^{2+} release channel on the internal sarcoplasmic reticulum (SR). To date, mechanisms underlying RyR2 dysregulation during diabetes remain poorly defined. A rat model of type 1 diabetes, in combination with echocardiography, *in vivo* and *ex vivo* hemodynamics, video edge-detection, confocal microscopy, Western blots, mass spectrometry, site-directed mutagenesis, [^{3}H]ryanodine binding, lipid bilayer and transfection assays were used to ascertain if post-translational modifications by reactive carbonyl species (RCS) are a contributing cause. After 8 weeks of diabetes, spontaneous Ca^{2+} release in ventricular myocytes increased ~5-fold. Evoked Ca^{2+} release from the SR was also non-uniformed (dyssynchronous). Total RyR2 protein remained unchanged, but its ability to bind the Ca^{2+}-dependent ligand [^{3}H]ryanodine was significantly reduced. Western blots and mass spectrometry revealed RCS adducts on select basic residues. Mutating residues to delineate the physiochemical impact of carbonylation yielded channels with enhanced and reduced cytoplasmic Ca^{2+}-responsiveness. The prototype RCS methylglyoxal (MGO) increased then decreased the open probability (P_o) of RyR2. MGO also increased spontaneous Ca^{2+} release and induced Ca^{2+} waves in healthy myocytes. Treating diabetic rats with RCS scavengers normalized spontaneous and evoked Ca^{2+} release from the SR, reduced carbonylation of RyR2, and increased binding of [^{3}H]ryanodine to RyR2. From these data we conclude that posttranslational modification by RCS is a contributing cause for heterogeneity in RyR2 activity seen during experimental diabetes.

Molecular Pharmacology Fast Forward. Published on May 30, 2012 as DOI: 10.1124/mol.112.078352
This article has not been copyedited and formatted. The final version may differ from this version.

INTRODUCTION

More than 350 million people worldwide have diabetes mellitus and ~70% of them will develop a unique type of heart failure referred to as diabetic cardiomyopathy (World Health Organization, 2011; American Diabetes Association, 2011). A significant percentage of these individuals will also succumb prematurely from a fatal stress-induced ventricular arrhythmia (American Diabetes Association 2011; Bertoni et al., 2004). To date, mechanisms responsible for the reduced basal and stress-induced aberrant ventricular contractions in individuals with diabetes mellitus remain incompletely defined and therapeutic strategies to slow their development/progression virtually non-existent.

Efficient and rhythmic ventricular contractions depend in part on adequate and synchronized release of Ca^{2+} from the sarcoplasmic reticulum (SR) via ryanodine receptor Ca^{2+} release channels (RyR2). Alterations in expression and/or function of RyR2 will reduce the rate and amplitude of Ca^{2+} release from the SR. Uncoordinated opening of RyR2 will also trigger delayed-after-depolarization and arrhythmias (Lehnart et al., 1998; Yano et al., 2009; Watanabe and Knollmann 2011).

Studies have reported either no change or a reduction in steady-state level of RyR2 protein during diabetes (Zhong et al., 2001; Netticadan et al., 2001; Bidasee et al., 2011; Bidasee et al., 2003a; Belke et al., 2004; Yaras et al., 2005; Ligeti et al., 2006; Periera et al., 2006). Increased spontaneous Ca^{2+} release has also been observed in ventricular myocytes isolated from streptozotocin (STZ)-induced diabetic rats, characteristic of enhanced cellular activity of RyR2 (Yaras et al., 2005; Shao et al., 2007). The latter was attributed in part to increased phosphorylation at RyR2 at Ser2808(9) and Ser2814(5) arising from enhanced protein kinase A and Ca^{2+}-calmodulin kinase II activities, and a reduction in the amount of the immunophilin

Molecular Pharmacology Fast Forward. Published on May 30, 2012 as DOI: 10.1124/mol.112.078352
This article has not been copyedited and formatted. The final version may differ from this version.

FKBP12.6 bound to RyR2 (Netticadan et al., 2001; Yaras et al., 2005; Shao et al., 2007; Shao et al., 2009). However, when RyR2 was isolated from diabetic rat hearts (dRyR2), its ability to bind the Ca^{2+}-dependent ligand [^{3}H]ryanodine was significantly reduced, consistent with a reduction in activity (Bidasee et al., 2003a; Shao et al., 2007). Electrically evoked Ca^{2+} release from the SR was also non-uniform (dyssynchronous) in diabetic myocytes (Shao et al., 2007), suggestive of uncoupling between L-type Ca^{2+} channels and RyR2. These paradoxical findings led us to propose the existence of two populations of RyR2 in diabetic myocytes; one population with enhanced Ca^{2+} responsiveness and another with reduced Ca^{2+} responsiveness, i.e., heterogeneity in the function of RyR2 during diabetes (Shao et al., 2007). Recently, dRyR2 was purified under reducing and dephosphorylating conditions, and using lipid bilayers we identified a population of channels with enhanced responsiveness to Ca^{2+}, ATP, cyclic ADP-ribose and reduced responsiveness to Mg^{2+} (Tian et al., 2011). The population of RyR2 with reduced Ca^{2+} responsiveness and mechanisms responsible for triggering heterogeneity in RyR2 function during diabetes remain to be characterized.

Reactive carbonyl species (RCS) are small electrophiles generated from glucose and fatty acid auto-oxidation, polyol pathway flux and by enzymes such as vascular adhesion protein-1/ serum semicarbazide-sensitive amine oxidase (Baynes and Thorpe 1999; Uchida 2000; Ellis 2007; Vander Jagt 2008). At low μM concentrations, RCS regulate cell proliferation, prevent aggregation of proteins, and tag proteins for degradation (Segré and Chiocca 2011; Wong et al., 2010; Barrera et al., 2004; Nagaraj et al., 2003; Dalle-Donne et al., 2006). During diabetes, production of RCS including lipid-derived malondialdehyde and 4-hydroxynonenal, and glucose-derived glyoxal, deoxyglucosone and methylglyoxal (MGO) increases (Vicentini et al., 2011; Fosmark et al., 2009; Slatter et al., 2004; Lapolla et al., 2005). These electrophiles will react with

Molecular Pharmacology Fast Forward. Published on May 30, 2012 as DOI: 10.1124/mol.112.078352
This article has not been copyedited and formatted. The final version may differ from this version.

susceptible basic amino acids on proteins to form RCS adducts. As far as we know, no enzymes have been identified in mammalian cells that are capable of breaking RCS adducts after they are formed on proteins. Therefore, RCS adducts formed on slowly turned over proteins like RyR2 ($t_{1/2}$ ~ 9 days, Ferrington et al., 1998) can be viewed as "diabetes-induced mutations."

Using matrix-assisted laser desorption ionization time-of-flight mass spectrometry (MALDI-TOF) and a Perl script, we earlier detected RCS adducts on RyR2 isolated from STZ-diabetic rat hearts (Bidasee et al., 2003). However, these adducts were not validated using other methodologies and their impact on RyR2 function was not characterized. The overarching hypothesis for the present study is that carbonylation (posttranslational modification by RCS) is an underlying cause for the heterogeneity in RyR2 activity seen during diabetes.

Molecular Pharmacology Fast Forward. Published on May 30, 2012 as DOI: 10.1124/mol.112.078352
This article has not been copyedited and formatted. The final version may differ from this version.

MATERIALS AND METHODS

Antibodies and Reagents

RyR2 antibodies were obtained from Thermo Fisher Scientific (Boulder, CO) and argpyrimidine antibodies were from JaiCA (Zhizuoka, Japan). N^{ε}-carboxy(methyl)lysine, 3-deoxyglycosone/imidazolone, GA-pyridine, pentosidine and pyrraline antibodies were supplied by Dr. Royji Nagai (Japan Women's University, Tokyo, Japan) and are now available through Cosmo Bio USA, Inc (Carlsbad, CA). [^{3}H]Ryanodine was purchased from GE Life Sciences (Boston, MA), phosphatidylserine, phosphatidylcholine, and phosphatidylethanolamine were obtained from Avanti Polar Lipids Inc. (Alabaster, AL), insulin pellets were from LinShin Canada Inc. (Scarborough, Canada) and pyridoxamine and aminoguanidine were from Sigma-Aldrich Chemical (Saint Louis, MO). MitoSOX® Red and MitoTracker® Green were obtained from Life Technologies (Grand Island, NY). Methylglyoxal (MGO) was synthesized, purified and quantified in our laboratory using the method described (Nemet et al., 2004). All other reagents used were of the highest grade commercially available.

Induction and verification of type 1 diabetes

Rats employed in this study were approved by the Institutional Animal Care and Use Committee, University of Nebraska Medical Center and adhered to the Guide for the Care and Use of Laboratory Animals (NIH Publication No. 85-23, National Research Council, 1996). Induction of diabetes using streptozotocin (STZ) and caring for type 1 diabetic rats were described in details previously (Shao et al., 2009, Tian et al., 2011).

Treatment of diabetic animals

Molecular Pharmacology Fast Forward. Published on May 30, 2012 as DOI: 10.1124/mol.112.078352
This article has not been copyedited and formatted. The final version may differ from this version.

Two weeks after injection of STZ (in 0.1 M citrate buffer, pH 4.5), diabetic rats were randomly divided into three groups. One group was administered pyridoxamine (Py) via drinking water for 5-6 weeks (Py-D, 1.6 g/kg/day, Shao et al., 2011), the second was given aminoguanidine (Ag, Ag-D, 1.6 g/kg/day, Shao et al., 2010) and the third remained untreated (D). Four weeks later, insulin pellets were implanted subcutaneous in some untreated diabetic animals to attain the euglycemic state (Ins-D). Two weeks after injection with citrate buffer, control animals were also divided into three groups: one group was administered pyridoxamine for 5-6 weeks (Py-C, 2.0 g/kg/day, as they drink one third less water than diabetic), the second with aminoguanidine (Ag-C, 2.0 g/kg/day) and the third remained untreated (C).

Blood parameters

Blood samples were collected via left renal arteries after anesthesia and assayed for glucose, insulin, thiobarbituric acid reactive substances (primarily lipid-derived malondialdehyde), serum semicarbazide-sensitive amine oxidase activity, methylglyoxal, (MGO, a glucose-derived RCS), and % glycosylated hemoglobin as described earlier (Shao et al., 2010; Shao et al., 2011).

Establishing diabetic cardiomyopathy (reduced ventricular function)

M-mode echocardiography was performed at the end of the 8-week protocol in anesthetized animals (100 mg/kg ketamine/2.5 mg/kg acepromazine, i.p.) to confirm reduced left ventricular function (*in vivo*) and a diabetic cardiomyopathy (Shao et al., 2010).

Establishing stress-induced aberrant ventricular contractions

Molecular Pharmacology Fast Forward. Published on May 30, 2012 as DOI: 10.1124/mol.112.078352
This article has not been copyedited and formatted. The final version may differ from this version.

Following euthanasia (Inactin® 75 mg/kg i.p.), chest cavities of control (C), diabetic (D) and insulin-treated diabetic (Ins-D) animals were opened, hearts were removed, mounted on a Langendorff apparatus via their aortas and perfused retrogradely with oxygenated Krebs-Henseleit buffer (118 mM NaCl, 27.2 mM $NaHCO_3$, 4.8 mM KCl, 1.2 mM $MgSO_4$, 1.0 mM KH_2PO_4, 1.25 mM $CaCl_2$ and 11 mM glucose, 37 ºC). A silk thread was then inserted through the apex of each ventricle and attached to a force displacement transducer (FT03C, Grass Instruments Company, West Warwick, RI USA) for measurement of developed ventricular tension (contraction). After stabilization, the right atrium of each heart was excised, atrioventricular node was crushed and a pair of platinum electrodes was inserted into the left ventricular wall to pace the ventricle at 180-200 beats per minute. Basal ventricular tension was determined. Isoproterenol (1 ml of 1 nM) was then injected via a side arm and changes in ventricular tension were determined. Hearts were allowed to stabilize for 30 min, a higher dose of isoproterenol (1 ml of 10 nM) was injected and changes in ventricular developed tension were determined.

Dyad junction architecture

Hearts were perfused retrogradely with Krebs-Henseleit buffer on a Langendorff apparatus to remove blood and then fixed with 3.5% glutaraldehyde in 1% phosphate buffered saline, pH 7.2. Left ventricles were cut into pieces, washed 3 times in 0.1M Sorenson's phosphate buffer saline (pH 7.3), post-fixed in 1% aqueous osmium tetroxide solution for 1hr at RT and washed 3 times with Sorenson's phosphate buffer saline. Tissues were then dehydrated in graded ethanol (50%, 70%, 90%, 95%, and 3 X 100%), followed by 3 X in 100% propylene oxide and then left overnight in a 1:1 mixture of propylene oxide and Araldite embedding medium. Ventricular

Molecular Pharmacology Fast Forward. Published on May 30, 2012 as DOI: 10.1124/mol.112.078352
This article has not been copyedited and formatted. The final version may differ from this version.

sections were then placed in flat silicon rubber molds with fresh Araldite and polymerized overnight at 65ºC. Ultrathin sections (~30–40 nm) were prepared with a Leica EM-UC 6 microtome (Leica Microsystems, Wien, Austria) using a Diatome diamond knife (Diatome, Biel, Switzerland) and stained in 2% uranyl acetate and Reynold's lead citrate. A transmission electron microscope (Philips 410LS operated at 80kV) was used to assess dyad junction architecture and the distance between T-tubule and junctional SR in a random manner.

Myocyte isolation and confirmation of altered sarcoplasmic reticulum (SR) Ca^{2+} release

Ventricular myocytes were isolated as described previously employing retrograde collagenase perfusion (Mitra and Morad, 1985; Shao et al., 2007). Confocal microscopy (whole cell and line-scan modes) was used to assess spontaneous and evoked Ca^{2+} releases in ventricular myocytes (Shao et al., 2007). Caffeine-induced Ca^{2+} transient amplitudes were also measured and used as indices of SR Ca^{2+} content (Shao et al., 2009).

Validation of and determining location of carbonyl adducts on RyR2

(a) Western blot:

Western blots employing membrane vesicles (30 μg) were used to determine relative levels of RyR2 protein in hearts from control, diabetic, insulin-treated and drug-treated animals (Shao et al., 2011; Tian et al., 2011). Western blots employing junctional sarcoplasmic reticulum vesicles (60 μg), prepared by fractionating membrane vesicles on discontinuous sucrose gradients (Tian et al., 2011) were also used to determine relative levels of argpyrimidine, N^{ε}-carboxy(methyl)lysine, 3-deoxyglycosone/hydroimidazolone, GA-pyridine, pentosidine and pyrraline adducts using

Molecular Pharmacology Fast Forward. Published on May 30, 2012 as DOI: 10.1124/mol.112.078352
This article has not been copyedited and formatted. The final version may differ from this version.

well–characterized antibodies (Ling et al., 1998; Oya et al., 1999; Nagai et al., 2003; Nagai et al., 2008). β-actin served as the internal control to correct for variations in sample loading.

(b) Mass Spectrometry

Immunoprecipitated RyR2 were solubilized in gel dissociation media and electrophoresed on 4-15% denaturing SDS-polyacrylamide gels, pre-run for 10 minutes prior to sample loading, for 180 min at 150V. Gels were then Coomassie-stained and destained with 30% methanol, and RyR2 bands were excised, digested with trypsin, desalted with ZipTips® (Millipore, Billerica, MA) and separated into two aliquots. One aliquot was subjected to matrix-assisted laser desorption ionization time-of-flight mass spectrometry (MALDI-TOF-MS) and data was searched for peptides with RCS adducts (Bidasee et al., 2003). The second aliquot was subjected to ESI-LC-MS/MS in a nanospray configuration using a microcapillary RP-C_{18} column (new Objectives, Woburn MA) to determine peptide sequence containing the RCS adduct. Tandem MS was performed with an ion trap mass spectrometer (LCQ-Deca XP Plus (Thermo Scientific, West Palm Beach, FL). Data-dependent acquisition was performed by carrying out a 1 sec survey scan between 380 and 1900 atomic mass unit (a.m.u.), followed by 2.4 sec MS/MS acquisition between 200 and 1300 a.m.u. Mascot Wizard was obtained from Matrix Science (http://www.matrixscience.com/).

Site-directed mutagenesis

Mutation studies (single and double) were conducted on the five amino acid residues to delineate the physiochemical effects of carbonylation: R1611 (between regions 1 and 2), K2190 and K2888 (within the middle region) and R4462 and R4683 (within the C-terminal). Mouse RyR2

Molecular Pharmacology Fast Forward. Published on May 30, 2012 as DOI: 10.1124/mol.112.078352
This article has not been copyedited and formatted. The final version may differ from this version.

cDNA (a gift from Dr. Wayne Chen, University of Alberta, CANADA) was excised from pcDNA3.0 using *Nhe*1 and *Not*1, purified using agarose gel electrophoresis and then restriction digested with *BsiW*I affording two fragments: *Nhe*1/*BsiW*I fragment (0-8864, fragment 1) and a *BsiW*I/*Not*1 fragment (8865-14904, fragment 2). Fragments were cloned in frame into pGEM-3z using their respective restriction sites, affording clone 1 (0-8864 bp) and clone 2 (8865-14904 bp), respectively. QuikChange™ mutagenesis kits (Stratagene, La Jolla, CA) were used to mutate R1611 and K2190 and K2888 (K2887 in mouse cDNA) in clone 1, and R4462 and R4683 (R4682 in mouse cDNA) in clone 2 to tyrosines and tryptophans. These residues were selected as they best reflected the charge neutralization and increase in bulk induced by RCS adducts. Glycine mutants were also created to assess the impact of charge neutralization only. Oligo primers of ~40 base pairs in length were used. After mutation, plasmids were transformed into competent HB101 cells, amplified in liquid cultures, purified using Maxi Prep columns (Qiagen, Valencia, CA) and mutations were confirmed using oligo sequencing. The fragments containing mutations were excised from pGEM-3z using appropriate restriction enzymes, purified from using agarose gel electrophoresis and ligated to the non-mutated fragment using T4-ligase (Promega, Madison WI) to create full length RyR2 containing respective mutation (s). Forward and reverse oligo sequencing was performed (mutation site and 4-5 random sites) to ensure that non-specific mutations did not occur during the procedures. Wild type and RyR2 mutant cDNAs were then cloned in frame into pCMS-EGFP (Clonetech, Mountain View, CA) using *Nhe*1 and *Not*1 restriction sites, transformed into competent HB101 cells, amplified in liquid broth and purified using plasmid Maxi Prep (Qiagen, Valencia, CA).

Expression of wild type and mutated RyR2

Molecular Pharmacology Fast Forward. Published on May 30, 2012 as DOI: 10.1124/mol.112.078352
This article has not been copyedited and formatted. The final version may differ from this version.

Wild type and RyR2 mutants (15-20 µg) were transfected into HEK-293T cells grown in Dulbecco Modified Eagle's Medium (DMEM) with 1.8 mM Ca^{2+} (>passage 10 and higher, 30-40% confluency, eighteen to twenty 100 mm dishes) using Ca^{2+}-phosphate (Chen and Okayama, 1987). These cells were chosen as they express little or no RyR2 (Luo et al., 2005). Media were changed 6-8 hrs after transfection and cells were allowed to grow for an additional 36-38 hrs. After this time cells were washed with 1 X phosphate buffered saline containing 1 mM EDTA, harvested by centrifugation (500 x g_{av} for 3 min), resuspended in buffer containing 0.25 M sucrose, 10 mM histidine, pH 7.3 and a protease inhibitor mix (1 mM benzamidine, 2 µg/ml leupeptin, 2 µg/ml pepstatin A, 2 µg/ml aprotinin, and 0.5 mM PMSF), and homogenized (5 X 6 sec using a Polytron setting 5). Homogenates were centrifuged (85,195 x g_{av} for 45 min) and membranes were collected, quick frozen in liquid nitrogen and stored at -80°C. Serial dilution Western blots were performed to determine RyR2 protein content in membrane vesicles.

Preparation of proteoliposomes containing RyR2

Proteoliposomes containing wild-type and RyR2 mutants were prepared as described earlier (Tian et al., 2011), except that 3.0 mg/ml of HEK-293T membranes were solubilized in 1.5% CHAPS. Proteoliposomes containing wild type and mutant RyR2 were stored in the vapor phase of liquid nitrogen until use.

Cytoplasmic Ca^{2+} responsiveness of wild type and RyR2 mutants

(a) [^{3}H]ryanodine binding assays

Membrane vesicles (0.1 mg/ml) were incubated in binding buffer (500 mM KCl, 20 mM

Molecular Pharmacology Fast Forward. Published on May 30, 2012 as DOI: 10.1124/mol.112.078352
This article has not been copyedited and formatted. The final version may differ from this version.

Tris·HCl, 5 mM reduced glutathione, and 100 μM EGTA, 6.7 nM [^{3}H]ryanodine, pH 7.4) with varying Ca^{2+} (0 to 4 mM) for 2 hr at 37°C. After incubation, membranes were filtered, washed, and the amount of [^{3}H]ryanodine bound to RyR2 was determined using liquid scintillation counting. Non-specific binding was determined simultaneously by incubating vesicles with 1 μM unlabeled ryanodine (Shao et al., 2007).

(b) Planar lipid bilayer assays

These studies were conducted as described recently (Tian et al., 2011). After fusion of RyR2 to the lipid bilayer, Ca^{2+} was added to the *cis* chamber and stirred vigorously for ~30 sec. Channel activity (open probability, gating and conductance) was then recorded for 6 minutes (3 min at +35mV and 3 min at -35 mV). Electrical signals were filtered at 2 kHz, digitized at 10 kHz, and analyzed using pClamp (Molecular Devices, Sunnyvale, CA). All experiments were carried out at room temperature (23–25°C) in ambient air.

(c) Transfection of wild type and RyR2 mutants into HEK-293T cells and responsiveness of cells to extracellular Ca^{2+}

Wild type RyR2, K2887W (a mutant with enhanced *cis* Ca^{2+} responsiveness), R4462Y (a mutant with reduced *cis* Ca^{2+} responsiveness) or a blank vector (pCMS-EGFP) was transfected into HEK-293T cells grown in DMEM using Ca^{2+} phosphate (Chen and Okayama, 1987). Media were changed 6-8 hr after transfection and cells were allowed to grow for an additional 36-38 hrs. Cells were then washed, loaded with Fura-2AM (5 μM) in low Ca^{2+} Tyrode solution (140 mM NaCl, 5.4 mM KCl, 1 mM Na_2HPO_4, 10 mM HEPES, 5 mM glucose, 1 mM $MgCl_2$, 0.2 mM Ca^{2+} pH 7.4) for 30 min at 37°C, placed on the stage of a Nikon microscope (TE2000) and

Molecular Pharmacology Fast Forward. Published on May 30, 2012 as DOI: 10.1124/mol.112.078352
This article has not been copyedited and formatted. The final version may differ from this version.

perfused with low Ca^{2+} Tyrode solution at a rate of 1.0 ml/min. Ca^{2+} concentration in perfusate was increased gradually to 0.4, 0.6, 1.0 and 1.8 mM (2.5 minutes each) and changes in cellular Ca^{2+} were recorded. Caffeine (10 mM) was added at the end to confirm functional RyR2 in cells assayed. Recordings were performed using dual excitation fluorescence photomultiplier system (Image Master Fluorescence Microscope, Photo Technology International USA) employing FELIX software (Photon Technology International). Cells were excited at 340/380 nm and emission measured at 510 nm.

Assessing effects of the RCS methylglyoxal (MGO) on RyR2 activity

(a) [^{3}H]ryanodine binding assays

Experiments were conducted as described above except that varying amounts of MGO (0 to 600 μM) were added to the binding buffer during incubation. In some experiments, membrane vesicles (0.1 mg/ml) were pre-incubated in binding buffer (500 mM KCl, 20 mM Tris·HCl, 13 μM Ca^{2+}, pH 7.4) with varying amounts of MGO (0 - 400 μM) for 30 min at 37°C. After this time, membranes were aliquoted into 10 tubes, 6.7 nM [^{3}H]ryanodine and increasing amounts of Ca^{2+} (0 to 4 mM) were added and incubation continued for 1.5 hr at 37°C. Membranes were filtered and washed, and the amount of [^{3}H]ryanodine bound was used as an index of the ability of MGO to modulate RyR2 activity.

(b) Lipid bilayer assays

Purified RyR2 from control animals were incorporated into lipid bilayer with 3.3 μM *cis* Ca^{2+}. MGO (0-80 μM) was added to the *cis* chamber and stirred vigorously for 30 sec. Channel activity (open probability, gating and conductance) was then recorded for 6 minutes (3 min at

Molecular Pharmacology Fast Forward. Published on May 30, 2012 as DOI: 10.1124/mol.112.078352
This article has not been copyedited and formatted. The final version may differ from this version.

+35mV and 3 min at -35 mV).

(c) Spontaneous and evoked Ca^{2+} release in myocytes

Ventricular myocytes isolated from control rats in DMEM F12 with 1.8 mM $CaCl_2$ were loaded with Fluo-3 AM for 30 min at 37°C. Cells were then washed, medium was replaced with Tyrode solution (140 mM NaCl, 5.4 mM KCl, 1 mM Na_2HPO_4, 10 mM HEPES, 5 mM glucose, 1.0 mM Ca^{2+}, 1 mM $MgCl_2$, pH 7.4) and chambers containing Fluo-3-loaded cells were placed on the stage of a laser confocal microscope (Nikon Swept Field confocal microscope equipped with a Cascade 512B high quantum efficiency digital camera and argon–krypton laser (5% intensity) and 60X plan Apo lens). Images of cells were collected every 2 sec, 3 ms per scan for 3 min to determine basal spontaneous Ca^{2+} release. MGO (25 μM) was then added and spontaneous Ca^{2+} release was assayed over 5 min. Experiments were also performed in line scan mode using a Zeiss 410 confocal microscope, field stimulating cells at 0.25 Hz (10 V for 10 ms) as described previously (Shao et al., 2009). Caffeine (10 mM) was added 6 min after addition of MGO to assess SR Ca^{2+} content.

Effects of MGO on mitochondrial production of superoxide and total reactive oxygen species (ROS)

Rat ventricular myocytes in DMEM F12, with 1.8 mM $CaCl_2$ were loaded with the mitochondria localizing probe MitoTracker® Green (100 nM) followed by the fluorogenic mitochondria-targeted superoxide/ROS probe MitoSOX® Red (2 μM) for 15 min each. After loading, DMEM was replaced with Tyrode solution (140 mM NaCl, 5.4 mM KCl, 1 mM Na_2HPO_4, 10 mM

Molecular Pharmacology Fast Forward. Published on May 30, 2012 as DOI: 10.1124/mol.112.078352
This article has not been copyedited and formatted. The final version may differ from this version.

HEPES, 5 mM glucose, 1.0 mM Ca^{2+}, 1 mM $MgCl_2$, pH 7.4) and cells were placed on the stage of a Zeiss LSM 510 Meta laser-scanning microscope with excitation at 405 nm (to detect superoxide-specific 2-hydroxyethidium product of oxidized MitoSOX® Red) and 488 nm (to detect ROS-produced ethidium products) wavelengths to capture fluorescent images for MitoTracker® Green and MitoSOX® Red, respectively. MitoTracker® Green was excited at 488 nM and emissions were monitored at 516 nm wavelength. MitoSOX® Red fluorescence was quantified using Image J analysis software.

Statistical Analysis

Differences among values from each of the groups (C, D, Ins-D, Py-C, Py-D, Ag-C, Ag-D and wild type and mutant RyR2) were evaluated using analysis of variance (ANOVA) employing GraphPad Prism. Data shown are means ± S.E.M. Results were considered significantly different if $p < 0.05$ (95% confidence interval).

Molecular Pharmacology Fast Forward. Published on May 30, 2012 as DOI: 10.1124/mol.112.078352
This article has not been copyedited and formatted. The final version may differ from this version.

RESULTS

General characteristics of animals used in the study

General characteristics of animals used in the study are shown in Table I. M-mode echocardiography confirmed reductions in ejection fraction and percent fractional shortening in diabetic animals. Insulin treatment reversed these changes indicating that changes in ejection fraction and percent fractional shortening resulted from the diabetes and not the diabetogenic agent STZ. Py and Ag treatments also blunted reductions in ejection fraction and fractional shortening. Insulin and Ag treatments blunted the increase in serum TBARS (malondialdehyde) while insulin, Py and Ag treatments blunted the increase in serum semicarbazide-sensitive amine oxidase activity induced by diabetes.

Ex vivo stress-induced aberrant ventricular contractions

Maximum developed tension (i.e., extent of contraction) in *ex vivo* diabetic hearts were 22.5 ± 3.5% less than that of control hearts (Fig. 1(i), left side). Isoproterenol-induced contractions (1 nM and 10 nM) were also significantly lower in diabetic rat hearts ($p < 0.05$). Treating diabetic animals with insulin for two weeks blunted these changes, emphasizing that reduction in ventricular contraction stemmed from the diabetes and not the diabetogenic agent STZ. When challenged with 10 nM isoproterenol, 56% (9 out of 16) of diabetic rat hearts also exhibited abnormal ventricular contractions compared with 13% of control hearts (2 out of 15, $p < 0.05$), Fig. 1(ii), red arrow. In 5 of these 9 diabetic hearts, normal contraction resumed within 10-30 sec after injection of 10 nM isoproterenol (Fig. 1(ii)). In the other 4 diabetic hearts rhythmic contraction ceased. Three out of 14 (21%) hearts from insulin-treated diabetic rats exhibited abnormal contractions when challenged with 10 nM isoproterenol. Two out of 16 diabetic, one of

Molecular Pharmacology Fast Forward. Published on May 30, 2012 as DOI: 10.1124/mol.112.078352
This article has not been copyedited and formatted. The final version may differ from this version.

15 control hearts and one out of 14 insulin-treated diabetic hearts tested exhibited abnormal contractions to 1 nM isoproterenol (p>0.05). These data are consistent with the notion that diabetic hearts are more likely to exhibit abnormal contractions when stressed (American Diabetes Association 2011; Bertoni et al., 2004).

Altered SR Ca^{2+} release in diabetic myocytes

(a) Spontaneous Ca^{2+} release (Ca^{2+} sparks)

Myocytes from hearts of diabetic animals exhibited a 4.8-fold higher frequency of spontaneous Ca^{2+} release from the SR compared with myocytes from controls (13.6 ± 1.2 sparks/50 µm/s *vs.* 2.8 ± 0.5 sparks/50 µm/s, $p < 0.05$, n ≥ 32 cells, ≥ 200 sparks from each group, Fig. 2(i)). There was no change in the full-width-at-half maximum between sparks from control and diabetic myocytes (2.10 ± 0.04 µm (D) *vs.* 2.05 ± 0.02 µm (C)). Insulin treatment blunted the increase in Ca^{2+} spark frequency, indicating that this defect stemmed from the diabetes and not from the diabetogenic agent, STZ. These data confirm earlier studies showing an increase in cellular activity of RyR2 in diabetic myocytes (Yaras et al., 2005; Shao et al., 2007).

(b) Evoked Ca^{2+} release

When field stimulated at 0.5Hz, the rate of evoked Ca^{2+} release from the SR and Ca^{2+} transient amplitude were reduced in diabetic myocytes compared with controls (78.2 ± 8.1 arbitrary fluorescence absorbance units (f.a.u.) (D) *vs.* 108.2 ± 5.2 f.a.u. (C); 3.3 ± 0.4 f.a.u. (D) *vs.* 4.8 ± 0.1 f.a.u. (C), Fig. 2(ii)). Ca^{2+} decay time was also significantly increased (722.1 ± 14.5 ms (D) *vs.* 260.5 ± 8.1 ms (C), Evoked Ca^{2+} release from the SR was also dyssynchronous (non-uniform) in more than 50% of myocytes from diabetic animals (Fig. 2(ii), middle white arrows),

Molecular Pharmacology Fast Forward. Published on May 30, 2012 as DOI: 10.1124/mol.112.078352
This article has not been copyedited and formatted. The final version may differ from this version.

with diastolic Ca^{2+} release in between pulses (green arrow). About 9% of diabetic myocytes exhibited Ca^{2+} alternans (Fig. 2(ii), middle panel). These data confirm non-uniform evoked release of Ca^{2+} from the SR (Shao et al., 2007).

Dyad junction architecture

Evoked Ca^{2+} release from the SR is dependent on the ability of L-type Ca^{2+} channels to respond to a depolarizing impulse, the spatial distance between T-tubules and SR membranes, and the responsiveness of RyR2 to influxed Ca^{2+}. A majority of studies have reported no change in L-type Ca^{2+} channel activity in myocytes from STZ-diabetic rats (Jourdon and Feuvray, 1993; Choi et al., 2002; Bracken et al., 2006; Shao et al., 2007). This prompted us to ascertain whether the spatial distance between T-tubules and SR membranes (i.e., the dyad junction architecture) is altered in myocytes from STZ-diabetic rats. Images collected randomly from the top, middle and apex of ventricles from C, D and Ins-D showed no significant difference in the distance between T-tubule and SR membranes (Fig. 2(iii)). The mean distance between SR and T-tubule membranes was 18.2 ± 4.8 nm in C, n = 103 images, 4 rats; 16.2 ± 3.4 nm in D, n = 122 images, 5 rats; and 17.7 ± 5.4 nm in Ins-D, n = 81 images, 4 rats. These new data indicate that the dyad junction architecture is not altered in myocytes from 8 weeks STZ-diabetic rats.

Reduced RyR2 activity during diabetes

With no change in activity of L-type Ca^{2+} channel and dyad junction architecture, we then focused our attention on RyR2. In this study, steady state levels of RyR2 protein did not change after 8 weeks of diabetes (Fig. 3(i), upper autoradiogram) but at equivalent amounts, dRyR2 protein bound ~30% less [^{3}H]ryanodine than cRyR2 at optimal Ca^{2+} (530.2 ± 12.3 fmol

Molecular Pharmacology Fast Forward. Published on May 30, 2012 as DOI: 10.1124/mol.112.078352
This article has not been copyedited and formatted. The final version may differ from this version.

[^{3}H]ryanodine/mg diabetic membranes compared with 762.2 ± 13.6 fmol [^{3}H]ryanodine/mg control membranes, $p < 0.05$, Fig. 3(i), graph below). Treatment with insulin blunted the reduction in [^{3}H]ryanodine binding to RyR2, confirming that this defect stems from diabetes and not from STZ. Interestingly, cRyR2, dRyR2 and RyR2 from insulin-treated animals (Ins-DRyR2) exhibited similar affinity for the prototype ligand ryanodine (K_d = 1.0 ± 0.1 nM for cRyR2, 0.8 ± 0.1 nM for dRyR2, and 0.9 ± 0.1 nM for Ins-DRyR2, p>0.05).

Increased carbonylation of RyR2 during diabetes

Compared with cRyR2, dRyR2 contained >2.5 times more immunoreactive N^{ϵ}-carboxy(methyl)lysine pyrraline, pentosidine, argpyrimidine, deoxyglucosone/hydroimidazole adducts, respectively, Fig. 3(ii) and Fig. 3(iii). Immunoreactive GA pyridine was found on dRyR2 but not detected on cRyR2. Insulin treatment blunted the levels of carbonyl adducts formed on RyR2.

Digestion of cRyR2, dRyR2 and Ins-DRyR2 with trypsin yielded 302, 251 and 281 peptides with M+H$^+$ values between 500 and 3000 Da, respectively. These peptides were within 10 ppm of theoretical RyR2 peptides and covered ~65% of its primary sequence. The PERL script designed to compare experimental masses (m/z) with theoretical digest masses (up to 3 miscleaved peptides) and search for modified peptides, generated a list of five peptides with RCS adducts on lysine or arginine residues. Fragmentation of these peptides using Tandem mass spectrometry confirmed they originated from RyR2. As an example, a single charged ion with m/z of 1202.60 was found following digestion of dRyR2 but not in cRyR2 or Ins-DRyR2 (Fig. 3(iv)). The PERL script predicted this mass is derived from glyoxal/methylglyoxal-derived hydroimidazolone on amino acid R4462 on peptide $_{4461}$L**R**QLTHTHR$_{4469}$. Fragmentation of this

Molecular Pharmacology Fast Forward. Published on May 30, 2012 as DOI: 10.1124/mol.112.078352
This article has not been copyedited and formatted. The final version may differ from this version.

peptide using Tandem mass spectrometry afforded b and y M+1 ions confirming the peptide $_{4461}$L**R**QLTHTHR$_{4469}$ (Fig. 3(v). We did not detect the imidazolone B adduct (142 Da) as it was below the set mass detection threshold. Since arginine is the only basic residue on this peptide where an imidazolone adduct can be formed, we reason that imidazolone B is on R4462. The combination of MALDI-TOF-MS, PERL script and Tandem MS/MS confirmed the locations of imidazolone B on R1611 ($_{1607}$VDVS**R**ISER$_{1615}$), pyrraline adducts on K2190 ($_{2185}$EITFP**K**MVANCCR$_{2197}$) and K2888 ($_{2887}$E**K**AQDILK$_{2892}$) in rat RyR2. In two experiments R4683 ($_{4675}$AALDFSDA**R**EK$_{4685}$) was modified with argpyrimidine and in two other experiments, R4683 was modified with hydroimizazolone. The carbonylation sites on RyR2 are similar to those in our prior study (Bidasee et al., 2003), but the adduct type was different on some residues.

Functional impact of carbonylation

We next set out to determine if RCS adducts are responsible for the functional heterogeneity of RyR2 seen during experimental type 1 diabetes mellitus. To date, chemical methods to insert a specific adduct on a defined amino acid residue without disrupting its tertiary structure of RyR2 are unavailable. Since carbonyl adducts neutralize basic charges and increases bulk, we reasoned that mutating these residues to tyrosines, tryptophans and glycines could provide insights into the roles these residues are playing in overall function of RyR2, and by extension extrapolate on the impact carbonylation of these residues would have on RyR2 function.

Three approaches were used to assess the activity of RyR2 mutants:

(a) Ca^{2+}-dependent binding of [^{3}H]ryanodine

Molecular Pharmacology Fast Forward. Published on May 30, 2012 as DOI: 10.1124/mol.112.078352
This article has not been copyedited and formatted. The final version may differ from this version.

Neutralizing the basic charge on R1611 by converting it to a glycine did not significantly alter Ca^{2+}-dependent binding of [^{3}H]ryanodine to RyR2 (Fig. 4(i)). Neutralizing the basic charge and increasing bulk on R1611 by converting it to a tryptophan and/or a tyrosine also did not alter the binding of [^{3}H]ryanodine (Fig. 4(i)). Neutralizing basic charges on K2190 or K2887 (the mouse equivalent of K2888) by converting each to a glycine also did not alter Ca^{2+}-dependent binding of [^{3}H]ryanodine (Fig. 4(ii) and Fig. 4(iii)). However, neutralizing the basic charge and increasing bulk on K2190 or K2887 by converting them to a tryptophan/tyrosine potentiated Ca^{2+}-dependent binding of [^{3}H]ryanodine to RyR2 (Fig. 4(ii) and Fig. 4(iii)). These increases in Ca^{2+}-dependent binding [^{3}H]ryanodine were not due to alterations in the amount of RyR2 protein used for assays (inset). Interestingly, R1611G/K2190Y, R1611W/K2190Y and K2190Y/K2887Y double mutants exhibited reduced ability to bind [^{3}H]ryanodine (Fig. 4(iv)). Neutralizing the basic charge or neutralizing charge and increasing bulk on residues R4462 and R4682 (the mouse equivalent of R4683) reduced binding of [^{3}H]ryanodine (Fig. 4(v) and Fig. 4(vi)).

(b) Planar lipid bilayer

To gain mechanistic insights underlying the altered [^{3}H]ryanodine binding, wild type and RyR2 mutants were purified, reconstituted into lipid bilayers and their gating and conductance were assayed as a function of *cis* (cytoplasmic) Ca^{2+}. Fig. 5(i) shows representative 1 second recordings of the *cis* Ca^{2+} responsiveness of wild type, single mutant (K2190Y, K2887W, R4462W and R4682G) and double mutant (R1611G/K2190Y, R1611W/K2190Y and K2190Y/K2887Y) at +35 mV, in 250 mM symmetric KCl. R1611 mutants were not assayed as they did not show alterations in Ca^{2+}-dependent [^{3}H]ryanodine binding. K2190Y and K2887W, which showed enhanced Ca^{2+}-dependent [^{3}H]ryanodine, were more responsive to low *cis* Ca^{2+}

Molecular Pharmacology Fast Forward. Published on May 30, 2012 as DOI: 10.1124/mol.112.078352
This article has not been copyedited and formatted. The final version may differ from this version.

(0.1 to 1 μM), as indicated by their increased open probabilities (Fig. 5(i), upper). The responsiveness of K2190Y was similar to that of wild type RyR2 at higher Ca^{2+}, but K2887W inactivated at lower Ca^{2+} ($EC_{50deactivation}$ = 20 μM compared with 3 mM for wild type RyR2, Fig. 5(ii). R1611G/K2190Y and R1611W/K2190Y and K2190Y/K2887Y double mutants showed reduced responsiveness to low and high *cis* Ca^{2+}, with channels. R4462W and R4682G mutants also exhibited reduced responsiveness to *cis* Ca^{2+} with channels, attaining maximum P_o of 0.42 and 0.37 with 1000 μM and 100 μM Ca^{2+}, respectively (Fig. 5(i) and Fig. 5(ii)).

In addition to alterations in *cis* Ca^{2+} responsiveness, the conductance of K2190Y, K2887W, R4462G and R4682W, R1611G/K2190Y and R1611W/K2190Y channels were also ~10% lower than that of wild type RyR2 (Fig. 5(iii), $p < 0.05$). The conductance of the double mutant K2190Y/K2887Y was similar to that of wild type RyR2 (Fig. 5(iii)).

(c) Transfection into HEK-293T cells and responsiveness to extracellular Ca^{2+}

We next set out to determine if mutant channels also exhibit altered Ca^{2+} responsiveness inside cells. Less than three percent of the ≥150 HEK-293T cells transfected with wild-type RyR2 showed intracellular Ca^{2+} oscillations in media containing 0.2 mM or 0.4 mM Ca^{2+} (Fig. 6(i) and Fig. 6(ii)). Increasing media [Ca^{2+}] to 1.0 mM or 1.8 mM only modestly increased intracellular Ca^{2+} oscillations in cells transfected with wild type RyR2 (8 out of 150 cells, 5%). Less than 3% of cells (4 out of 149 cells) transfected with R4462Y, a mutant with reduced *cis* Ca^{2+} responsive, exhibited intracellular Ca^{2+} oscillation in media with [Ca^{2+}] ranging from 0.2 to 1.8 mM (Fig. 6(i) and Fig. 6(ii)). However, cells transfected with K2887W, a mutant with enhanced Ca^{2+} responsiveness, exhibited enhanced Ca^{2+} oscillations in low and high media Ca^{2+} (9 out of 154 cells (6%) in 0.2 mM Ca^{2+}; 25 out of 154 cells (16%) in 0.6 mM Ca^{2+}; 35 out of 154 cells

Molecular Pharmacology Fast Forward. Published on May 30, 2012 as DOI: 10.1124/mol.112.078352
This article has not been copyedited and formatted. The final version may differ from this version.

(23%) in 1.8 mM Ca^{2+}). All cells assayed generated Ca^{2+} transients when challenged with 10 mM caffeine, indicating that they contained functional RyR2. These data strongly suggest that carbonylation can induce aberrant opening and/or closing of RyR2 inside myocytes.

RCS modulate RyR2 and trigger Ca^{2+} release from the SR

We then proceeded to determine if RCS can also alter the activity of RyR2 *in vitro*. The prototype RCS chosen for this study was MGO.

(a) Effect of MGO binding of [^{3}H]ryanodine to RyR2

In competition [^{3}H]ryanodine binding assays conducted in 300 μM free cytoplasmic Ca^{2+}, MGO initially enhanced, then displaced ryanodine from RyR2 in two phases. The $K_{i(1)}$ for phase A displacement was 25.0 ± 2.5 μM and the $K_{i(2)}$ for phase B displacement was 400.5 ± 10.2 μM (Fig. 7(i)). Not surprisingly, the displacement curve for MGO was not parallel to that of ryanodine (data not shown), suggesting that MGO and ryanodine are interacting at different sites on RyR2. In a more extensive study, we found that pre-treating membrane vesicles with 15 μM MGO for 30 min enhanced the amount of [^{3}H]ryanodine bound to RyR2 at all Ca^{2+} concentrations tested (Fig. 7(ii)). Pre-treatment with 200 μM and 400 μM MGO also enhanced binding of [^{3}H]ryanodine to RyR2 at lower Ca^{2+} (0.1 to 13 μM) but reduced [^{3}H]ryanodine at higher Ca^{2+} (70 to 3900 μM, Fig. 7(ii)).

(b) Lipid bilayer assays

To gain mechanistic insights, purified RyR2 were reconstituted into lipid bilayers and the effects of MGO on gating and conductance were determined. Addition of 16 μM MGO to the *cis*

Molecular Pharmacology Fast Forward. Published on May 30, 2012 as DOI: 10.1124/mol.112.078352
This article has not been copyedited and formatted. The final version may differ from this version.

chamber of the lipid bilayer chamber (3.3 μM *cis* Ca^{2+}, 250 mM symmetric KCl, +35 mV) increased the open probability of RyR2 (P_o increased from 0.21 to 0.51, $p < 0.05$, Fig. 7(iii) and Fig. 7(iv)) within 1 min after addition. The increase in P_o was seen at both positive and negative holding potentials and resulted predominantly from an increase in the dwell time in the open state (dwell time increased from 1.5 ms to 5.7 ms, $p < 0.05$). Increasing MGO concentration in the *cis* chamber further (32 μM to 80 μM) dose-dependently reduced the P_o of RyR2 from 0.51 to 0.05 (Fig. 7(iii) and Fig. 7(iv)). Concentrations of MGO >40 μM also significantly ($p < 0.05$) reduced the conductance of RyR2 (Fig. 7(iii) and Fig. 7(iv)).

(c) MGO effects on Ca^{2+} release from the SR

[^{3}H]ryanodine and lipid bilayer assays indicated that MGO alters the responsiveness of RyR2 to cytoplasmic Ca^{2+}. We then sought to determine if MGO can also alter the activity of RyR2 inside cardiac myocytes. Time-lapse images from one of 24 quiescent myocytes exposed to MGO are shown in Fig. 8(i). Ten sec after addition of MGO (25 μM), spontaneous Ca^{2+} release increased in random locations within the myocyte (red arrows). This increase in spontaneous Ca^{2+} release persisted anywhere from 37 to 45 sec depending on the cell, and then transitioned into a Ca^{2+} wave that lasted for about 2.5 sec, triggering myocyte contraction. Nuclear Ca^{2+} also increased following the Ca^{2+} wave (white arrows). Removal of media Ca^{2+} did not alter MGO's ability to alter spontaneous Ca^{2+} release and generation of Ca^{2+} waves (data not shown), indicating that MGO was triggering release of Ca^{2+} from the SR.

Line scan studies were also conducted with 0.25 Hz field stimulation. Within 15 sec after addition of MGO (20 μM), spontaneous Ca^{2+} release from the SR increased 12.8-fold in 18 of 22 of myocytes (Ca^{2+} spark frequency before addition of MGO was 1.8 ± 0.5 sparks/50 μm/s *vs* 21.6

Molecular Pharmacology Fast Forward. Published on May 30, 2012 as DOI: 10.1124/mol.112.078352
This article has not been copyedited and formatted. The final version may differ from this version.

± 1.2 sparks/50 µm/s after MGO addition, $p < 0.05$, Fig. 8(ii)). The increase in Ca^{2+} spark frequency continued for 30 ± 6 sec. In 66% of myocytes (12 of 18 cells), Ca^{2+} sparks transitioned into Ca^{2+} waves as shown in Fig. 8(ii). These Ca^{2+} waves reduced the amplitude of evoked Ca^{2+} transient (from $\Delta F = 4.8 \pm 0.4$ f.a.u. after MGO but before the wave, $\Delta F = 4.0 \pm 0.2$ f.a.u after MGO and after wave). Evoked Ca^{2+} release from the SR following MGO treatment was dyssynchronous, akin to that seen in diabetic myocytes (white arrows, Fig. 7(ii)). Spontaneous and evoked Ca^{2+} cycling ceased in 18 out of 22 cells (80%), five-minutes after the addition of MGO. Addition of caffeine (10 mM) to myocytes after cessation of evoked Ca^{2+} transients triggered Ca^{2+} release from the SR, but the amplitude was significantly reduced (31.9 ± 7.7% of that generated in untreated myocytes, n = 8 cells).

Effect of MGO on mitochondria production of superoxide/reactive oxygen species

Previous studies have shown that MGO increases mitochondrial superoxide/ROS production (Du et al., 2001). Time-lapsed confocal microscopy was then used to ascertain whether changes in intracellular Ca^{2+} homeostasis induced by MGO resulted from MGO's direct action on RyR2 or from the superoxide/ROS it produces acting on RyR2. Addition of MGO (20 µM) to freshly isolated rat ventricular myocytes (n = 16 cells) increased mitochondrial superoxide ($O_2^{\bullet}$) and total ROS production. However, this increase started ~8-9 minutes after the addition of MGO (Fig. 9(i) and Fig. 9(iv)). Analyses of Z-stack images of mitochondria (Mitotracker® Green), mitochondria $O_2^{\bullet}$ (405 nm excitation of MitoSOX®) and mitochondria total ROS (488 nm excitation of MitoSOX®), before and after MGO addition revealed a 210.5 ± 6.4% (n = 7) increase in $O_2^{\bullet}$ fifteen minutes after addition of MGO (Fig. 9(ii) and Fig. 9(iii)), and a 758.9 ± 12.2% (n=7) in total ROS sixteen minutes after MGO addition (Fig. 9(vi) and Fig. 9(vii)).

Molecular Pharmacology Fast Forward. Published on May 30, 2012 as DOI: 10.1124/mol.112.078352
This article has not been copyedited and formatted. The final version may differ from this version.

Increasing MGO to 40 μM, shortened the time to detection of mitochondrial $O_2^{\bullet}$ and total ROS production to ~3 minutes and the amount of $O_2^{\bullet}$ and total ROS produced by 50% (data not shown).

Treatment with scavengers of RCS blunts RyR2 dysregulation

Earlier we reported that treatment of diabetic rats with RCS scavengers, aminoguanidine (Ag) and pyridoxamine (Py) blunted reductions in cardiac and myocyte function (Shao et al., 2010, 2011). These drugs did not alter blood serum glucose levels, but decreased serum SSAO activity and thiobarbituric acid reactive substances (principally malondialdehyde, Table 1). In this study, treating diabetic rats with Py and Ag also blunted the increase in Ca^{2+} spark frequency (Fig. 10(i)). Py and Ag treatments prevented formation of carbonyl adducts on RyR2 (Fig. 10(ii) and Fig. 10 (iii)); Py treatment reduced N^{ε}-carboxy(methyl)lysine adduct by 79.2 ± 5.1%, pentosidine adduct by 86.4 ± 8.2%, pyrraline adduct by 88.3 ± 12.1% and 3-deoxyglucosone/hydroimidazole by 89.1 ± 11.2%. Ag treatment was less effective, reducing N^{ε}-carboxy(methyl)lysine adduct by 48.1 ± 7.2%, pentosidine adduct by 38.1 ± 9.1%, pyrraline adduct by 67.1 ± 9.1% and 3-deoxyglucosone/hydroimidazole by 58 ± 13% (Fig. 10(iii)). Py and Ag-treatments did not alter expression of RyR2 during diabetes but enhanced its ability to bind [^{3}H]ryanodine (Fig. 10(iv), graph). The amplitude of caffeine-induced Ca^{2+} transients in diabetic myocytes was 52% less than that of control myocytes (ΔF= 0.37 ± 0.02 f.a.u. compared to 0.76 ± 0.03 f.a.u.). Py and Ag-treatments blunted the reduction in caffeine-induced Ca^{2+} transient amplitude to 80.2 ± 3.4 % and 74.5 ± 4.5 of controls, respectively (Fig. 10(v)).

Molecular Pharmacology Fast Forward. Published on May 30, 2012 as DOI: 10.1124/mol.112.078352
This article has not been copyedited and formatted. The final version may differ from this version.

DISCUSSION

The principal finding of the present study is that the heterogeneity in RyR2 function seen in hearts of STZ-induced diabetic rats stems in part from post-translational modification by RCS. These modifications alter the sensitivity of RyR2 to cytoplasmic Ca^{2+}, with some modifications enhancing cytoplasmic Ca^{2+} responsiveness, while others reduces the responsiveness of the channel to cytoplasmic Ca^{2+}. In this study carbonyl adducts were confirmed on five amino acid residues of RyR2. These residues are by no means the complete list of amino acids on RyR2 that undergo carbonylation during diabetes. Elevated levels of pentosidine, N^{ϵ}-carboxy(methyl)lysine and GA pyridine adducts were detected on dRyR2 using Western blot assays but their locations on RyR2 were not determined. Several reasons for the latter are likely, including reduced ionization efficiency of the carbonylated peptides, the inability of our PERL algorithm to efficiently locate cross-linking pentosidine adducts and some adducts may be formed at relatively low levels (Ahmed et al., 2003). Another reason could be the method itself. In the present study, trypsin was used for digestion of RyR2. This enzyme cleaves at lysines and arginines and if a modification is present on either residue, trypsin will not digest. Had GluC which cleaves at glutamyl residues been used for digestion of RyR2, more peptides with carbonyl adducts may have been obtained (Priego-Capote and Sachez 2009).

A surprising finding of the present study is that RCS did not indiscriminately react with all available basic amino acid residues on RyR2. Some residues are more susceptible to carbonylation (like the ones identified) than others. One reason for this could be the electronic environment of these residues. Basic residues with low $pK_{a's}$ are more likely to undergo carbonylation than residues with higher $pK_{as'}$, since a higher fraction of the low pK_a residue will

Molecular Pharmacology Fast Forward. Published on May 30, 2012 as DOI: 10.1124/mol.112.078352
This article has not been copyedited and formatted. The final version may differ from this version.

exist in the deprotonated state at a physiological pH of 7.4 rendering it susceptible to modification (Iberg and Flückiger, 1986) .

The present study also indicates that the site and extent of modification dictates the effects carbonylation on RyR2 function. In this study mutating R1611 had no significant impact on RyR2 function. This finding raises the possibility that some residues are acting as "sinks" to protect RyR2 from transient burst in α-oxoaldehydes production that may occur. On the other hand, mutations at K2190 or K2887 exaggerated Ca^{2+} responsiveness of RyR2. In the resting or non-activated state, the N-terminal and central domains of RyR2 make close contacts at several regions to maintain RyR2 in a closed state. Two such subdomains reside between amino acids 2000-2500 (Ikemoto and Yamamoto, 2002) and 2234 and 2750 (Suetomi et al., 2011). Since K2190 and K2887 reside on either side of these domains, we speculate that these residues may be involved in "domain zipping", and modifying them may destabilize N-terminal domain-C-terminal interactions, leading to enhanced Ca^{2+} responsiveness of RyR2.

Mutagenesis studies also suggest that carbonylation at R4462 or R4682 will likely reduced the Ca^{2+} responsiveness of RyR2. These residues reside within and immediately downstream of divergent region 1 (amino acids 4254 and 4631), which dictates Ca^{2+} sensitivity of RyR (Du et al., 2000) and increasing bulk on these residues could compromise the ability of Ca^{2+} to activate RyR2.

Our data also showed that mutations at more than one sites (R1611, K2190 and K2887) reduced the Ca^{2+} responsiveness of RyR2 (Fig. 4), suggesting that the more extensive the carbonylation, the more likely RyR2 activity will be reduced. More extensive carbonylation will occur from increased duration of diabetes and/or from higher glucose levels (more glucose-derived RCS generated). Since blood glucose levels of 15 week db/db mice are >30 mmol,

Molecular Pharmacology Fast Forward. Published on May 30, 2012 as DOI: 10.1124/mol.112.078352
This article has not been copyedited and formatted. The final version may differ from this version.

increased carbonylation of RyR2 may be a contributing cause for reduced frequency of in Ca^{2+} sparks reported myocytes from db/db type 2 diabetic mice (Periera et al., 2006). Factors other than high levels of glucose may also be at play to reduce the activity of RyR2 (Lacombe et al., 2007).

Using Western blots, a 2 to 5 fold increase in carbonyl adducts was found on dRyR2. These are aggregate increases and do not indicate the extent to which individual RyR2 molecule are modified by RCS, and how much of the total RyR2 protein in the cell undergoes carbonylation during diabetes. What we do know from [^{3}H]ryanodine binding studies is ~30% of total dRyR2 exhibited reduced Ca^{2+} responsiveness. The amount of RyR2 with enhanced Ca^{2+} responsiveness is not known, but we suspect that it may be significant as the majority of channels assayed in an earlier study exhibited gain-of-function (Tian et al., 2011). It is also important to appreciate that more than one type of carbonyl adducts can be found on a susceptible amino acid residue during diabetes. For example, in this study both imidazolone A/B (derived from glyoxal/methylglyoxal) and argpyrimidine (derived from MGO) were found on R4462 of RyR2. Which type of adduct is formed on any give residue may be dictated by the concentration of RCS present.

It has been known for more than twenty years that RCS and RCS-adducts are elevated in serum of individuals with diabetes (Makita et al., 1992; Slatter et al., 2004; Lapolla et al., 2005; Fosmark et al., 2009; Vicentini et al., 2011) and that scavengers of RCS can prevent diabetic complications (Brownlee et al., 1986). Although RCS-adduct breaking strategies have been not been successful in clinical studies (Hartog et al., 2011), therapies involving agents that scavenge and/or preventing RCS production have (Bolton et al., 2004, Williams et al., 2007). These drugs are likely exerting their beneficial effects through multiple mechanisms, including chelating

Molecular Pharmacology Fast Forward. Published on May 30, 2012 as DOI: 10.1124/mol.112.078352
This article has not been copyedited and formatted. The final version may differ from this version.

metals involved in the synthesis of RCS (Nagai et al., 2102). In this study we found that Py was also more effective than Ag in reducing carbonylation of and normalizing the Ca^{2+} responsiveness (activity) of RyR2. Could it be that Py is more efficacious than Ag because of its lower primary amine content allows it to enter myocytes? If this is the case, then cellular permeability may be an important consideration when designing RCS-reducing therapies. It should be pointed out that in a recent study we found that in addition to elevation in serum, glucose-derived MGO and the enzyme that synthesizes it vascular adhesion protein-1/serum semicarbazide amine oxidase were also upregulated in ventricular myocytes (Shao et al., 2011). We also found MGO-derived argpyrimidine adduct on SERCA2 (Shao et al., 2011) and on RyR2 (Fig. 3(ii)), despite an increase in expression of glyoxalase-1 (Glo-1), the enzyme that degrades glucose-derived α-oxoaldehydes.

The present study is not without limitations. First, none of the mutants created are ideal to mimic the simultaneous charge neutralization and increase in bulk induced by carbonylation. Tryptophan has a hydrophobic side chain which could compromise protein folding and tyrosine is a phosphorylatable residue which could alter RyR2 activity. Although alanine (maybe isoleucine/leucine) would have been a more appropriate choice than glycine to mimic charge neutralization, we were fortunate in that the characteristics of our glycine mutants parallel those of the corresponding tryrosines and tryptophans.

Second, we and others have shown that SERCA2 activity is reduced in the myocardium during diabetes (Shao et al., 2011; Belke et al., 2004). In addition to affecting the rate and amount of Ca^{2+} transported from the cytoplasm to the lumen of the SR (i.e. SR Ca^{2+} content), a reduction in SERCA2 will elevate diastolic Ca^{2+} which in turn can increase the activity of RyR2. In a recent study we found that SERCA2 is also extensively modified by RCS during diabetes

Molecular Pharmacology Fast Forward. Published on May 30, 2012 as DOI: 10.1124/mol.112.078352
This article has not been copyedited and formatted. The final version may differ from this version.

and that treatment of diabetic rats with Py prevented carbonylation of SERCA2, and enhance its activity (Shao et al., 2011). Thus, the increase in Ca^{2+} sparks seen in diabetic myocytes and the reduction in Ca^{2+} sparks seen in myocytes from Py and Ag-treated rats may also be due in part to a reduction in SERCA2 activity.

Third, in addition to regulation by cytoplasmic Ca^{2+}, the activity of RyR2 is also regulated by an array of other cytoplasmic ligands and proteins and by luminal $Ca^{2+.}$ Whether these carbonylation-mimicking RyR2 mutants altered the responsiveness of RyR2 to activating/deactivating ligands such as ATP, cADP-ribose and Mg^{2+} and whether these mutants exhibit altered luminal Ca^{2+} responsiveness remains to be determine. It is also not clear whether RCS adducts are altering the binding of proteins to RyR2 including FKBP12.6, PP2a and calmodulin.

Fourth, it is unlikely that MGO increases Ca^{2+} sparks in myocytes solely from its action on RyR2. MGO also acts on SERCA2 which can affect RyR2 activity. It is also possible that MGO may be altering the redox status of the mitochondria which directly impacts the activity of RyR2 (Zhou et al., 2011). However, based on the findings of the present study, MGO's action on the mitochondria occurs after that on SR Ca^{2+} cycling proteins. MGO was used as a prototype RCS and its effects on intracellular Ca^{2+} homeostasis and RyR2 function occurred very fast (sec to min). Although this rapid modification with MGO emphasizes our point that RyR2 is a molecular target, we do not have any data on the kinetics of action of other RCS such as malondialdehyde, 4-hydroxynonenal and glucosone.

In conclusion, this study identifies carbonylation as a novel mechanism that contributes to RyR2 dysregulation (functional heterogeneity) during diabetes. Limited carbonylation enhances or reduces cytoplasmic Ca^{2+} responsiveness of RyR2 (depending on the site of carbonylation),

Molecular Pharmacology Fast Forward. Published on May 30, 2012 as DOI: 10.1124/mol.112.078352
This article has not been copyedited and formatted. The final version may differ from this version.

while extensive carbonylation reduces the cytoplasmic Ca^{2+} responsiveness of RyR2. Aberrant opening of RyR2 resulting from enhanced Ca^{2+} responsiveness will induce delayed after depolarization and arrhythmias (Lehnart et al., 1998; Marks 2002; Watanabe and Knollmann 2011), while decreased Ca^{2+} responsiveness of RyR2 will reduce the amplitude of evoked Ca^{2+} release from the SR and muscle contraction, phenotypes that are commonly seen in individuals with diabetes mellitus. Reducing RCS levels also blunted RyR2 dysregulation during diabetes. Collectively, these new data suggest that myocyte-permeant RCS scavengers may be useful as an adjunct therapy for slowing the development of heart failure in individuals with diabetes.

Molecular Pharmacology Fast Forward. Published on May 30, 2012 as DOI: 10.1124/mol.112.078352
This article has not been copyedited and formatted. The final version may differ from this version.

ACKNOWLEDGEMENTS

The authors thank Dr. Clara Franzini-Armstrong (University of Pennsylvania) for assistance with electron microscopic studies of dyad junctions, Dr. Wayne Chen (University of Calgary) for providing mouse cDNA encoding RyR2, Dr. Gerhard Meissner (University of North Carolina) for assistance with bilayer set up and Dr. Mu Wang (Indiana University School of Medicine) for assistance with early mass spectrometry analyses. We also thank Janice A. Taylor and James R. Talaska of the Confocal Laser Scanning Microscope Core Facility at the University of Nebraska Medical Center for providing assistance with confocal microscopy.

Molecular Pharmacology Fast Forward. Published on May 30, 2012 as DOI: 10.1124/mol.112.078352
This article has not been copyedited and formatted. The final version may differ from this version.

AUTHORS CONTRIBUTION

Participated in research design: Bidasee, Singh and Rozanski

Conducted experiments: Shao, Tian, Ouyang, Moore, Bidasee, and Alomar, D'Souza

Contributed new reagents or analytic tools: Nagai and Nemet

Performed data analysis: Bidasee, Shao, Tian, Ouyang, Moore, Alomar, Kutty and Ramanadham.

Wrote or contributed to the writing of the manuscript: Bidasee, Rozanski, Singh, Moore, Kutty, and Ramanadham.

Molecular Pharmacology Fast Forward. Published on May 30, 2012 as DOI: 10.1124/mol.112.078352
This article has not been copyedited and formatted. The final version may differ from this version.

REFERENCES

Ahmed N, Thornalley PJ, Dawczynski J, Franke S, Strobel J, Stein G, and Haik GM (2003) Methylglyoxal-derived hydroimidazolone advanced glycation end-products of human lens proteins. I*nvest Ophthalmol Vis Sci* **44(12)**: 5287-5292.

American Diabetes Association. Living with Diabetes: Complications. http://www.diabetes.org/living-with-diabetes/complications/ (accessed May 6th 2012).

Barrera G, Pizzimenti S, and Dianzani MU (2004) 4-hydroxynonenal and regulation of cell cycle: effects on the pRb/E2F pathway. *Free Radic Biol Med* **37(5)**: 597-606.

Baynes JW, and Thorpe SR (1999) Role of oxidative stress in diabetic complications: a new perspective on an old paradigm. *Diabetes* **48(1)**: 1-9.

Belke DD, Swanson EA, and Dillmann WH (2004) Decreased sarcoplasmic reticulum activity and contractility in diabetic db/db mouse heart. *Diabetes* **53(12)**: 3201-3208.

Bertoni AG, Hundley WG, Massing MW, Bonds DE, Burke GL, and Goff DC Jr (2004) Heart failure prevalence, incidence, and mortality in the elderly with diabetes. *Diabetes Care* **27**: 699-703.

Bidasee KR, Dinçer UD, and Besch HR Jr (2001) Ryanodine receptor dysfunction in hearts of streptozotocin-induced diabetic rats. *Mol Pharmacol* **60(6)**: 1356-1364.

Bidasee KR, Nallani K, Yu Y, Cocklin RR, Zhang Y, Wang M, Dincer UD, and Besch HR Jr (2003) Chronic diabetes increases advanced glycation end products on cardiac ryanodine receptors/calcium-release channels. *Diabetes* **52(7)**: 1825-1836.

Bolton WK, Cattran DC, Williams ME, Adler SG, Appel GB, Cartwright K, Foiles PG, Freedman BI, Raskin P, Ratner RE, Spinowitz BS, Whittier FC, and Wuerth JP for the ACTION I Investigator Group (2004) Randomized Trial of an Inhibitor of Formation of Advanced Glycation End Products in Diabetic Nephropathy *Am J Nephrol* **24**: 32–40.

Bracken N, Howrath FC, and Singh J (2006) Effects of streptozotocin-induced diabetes on contraction and calcium transport in rat ventricular cardiomyocytes. *Ann N Y Acad Sci* **1084**: 208-222.

Brownlee M, Vlassara H, Kooney A, Ulrich P, and Cerami A (1986) Aminoguanidine prevents diabetic-induced arterial wall protein cross-linking. *Science* **232(4758)**: 1629-1632.

Chen C, and Okayama H (1997) High-efficiency transformation of mammalian cells by plasmid DNA. *Mol Cell Biol* **7(8)**: 2745-2752.

Choi KM, Zhong Y, Hoit BD, Grupp IL, Hahn H, Dilly KW, Guatimosim S, Lederer WJ, and Matlib MA (2002) Defective intracellular Ca^{2+} signaling contributes to cardiomyopathy in Type 1 diabetic rats. *Am J Physiol Heart Circ Physiol* **283(4)**: H1398-H1408.

Dalle-Donne I, Aldini G, Carini M, Colombo R, Rossi R, and Milzani A (2006) Protein carbonylation, cellular dysfunction, and disease progression. *J Cell Mol Med* **10(2)**: 389-406.

Du GG, Khanna VK, and MacLennan DH (2000) Mutation of divergent region 1 alters caffeine and Ca(2+) sensitivity of the skeletal muscle Ca^{2+} release channel (ryanodine receptor). *J Biol Chem* **275(16)**: 11778-11783.

Du J, Suzuki H, Nagase F, Akhand AA, Ma XY, Yokoyama T, Miyata T, and Nakashima I (2001) Superoxide-mediated early oxidation and activation of ASK1 are important for initiating methylglyoxal-induced apoptosis process. *Free Radic Biol Med* **31(4)**: 469-478.

Ellis EM (2007) Reactive carbonyls and oxidative stress: potential for therapeutic intervention. *Pharmacol Ther* **115(1)**: 13-24.

Ferrington DA, Krainev AG, and Bigelow DJ (1998) Altered turnover of calcium regulatory proteins of the sarcoplasmic reticulum in aged skeletal muscle. *J Biol Chem* **273(10)**: 5885-5891.

Fosmark DS, Berg JP, Jensen AB, Sandvik L, Agardh E, Agardh CD, and Hanssen KF (2009) Increased retinopathy occurrence in type 1 diabetes patients with increased serum levels of the advanced glycation endproduct hydroimidazolone. *Acta Ophthalmol* **87(5)**: 498-500.

Hartog JW, Willemsen S, van Veldhuisen DJ, Posma JL, van Wijk LM, Hummel YM, Hillege HL, Voors AA, and BENEFICIAL investigators (2011) Effects of alagebrium, an advanced glycation endproduct breaker, on exercise tolerance and cardiac function in patients with chronic heart failure. *Eur J Heart Fail* **13(8)**: 899-908.

Iberg N, and Flückiger R (1986) Nonenzymatic glycosylation of albumin in vivo. Identification of multiple glycosylated sites. *J Biol Chem* **261(29)**:13542-13545.

Ikemoto N, and Yamamoto T (2002) Regulation of calcium release by interdomain interaction within ryanodine receptors. *Front Biosci* **7**: d671–d683.

Jourdon P, and Feuvray D (1993) Calcium and potassium currents in ventricular myocytes isolated from diabetic rats *J Physiol* **470**: 411–429.

Lacombe VA, Viatchenko-Karpinski S, Terentyev D, Sridhar A, Emani S, Bonagura JD, Feldman DS, Györke S, and Carnes CA (2007) Mechanisms of impaired calcium handling underlying subclinical diastolic dysfunction in diabetes. *Am J Physiol Regul Integr Comp Physiol* **293(5)**: R1787-R1797.

Lapolla A, Flamini R, Lupo A, Aricò NC, Rugiu C, Reitano R, Tubaro M, Ragazzi E, Seraglia R, and Traldi P (2005) Evaluation of glyoxal and methylglyoxal levels in uremic patients under peritoneal dialysis. *Ann N Y Acad Sci* **1043**: 217-224.

Lehnart SE, Schillinger W, Pieske B, Prestle J, Just H, and Hasenfuss G (1998) Sarcoplasmic reticulum proteins in heart failure. *Ann N Y Acad Sci* **853**: 220-230.

Ligeti L, Szenczi O, Prestia CM, Szabó C, Horváth K, Marcsek ZL, van Stiphout RG, van Riel NA, Op den Buijs J, Van der Vusse GJ, and Ivanics T (2006) Altered calcium handling is an early sign of streptozotocin-induced diabetic cardiomyopathy. *Int J Mol Med* **17(6)**: 1035-1043.

Ling X, Sakashita N, Takeya M, Nagai R, Horiuchi S, and Takahashi K (1998). Immunohistochemical distribution and subcellular localization of three distinct specific molecular structures of advanced glycation end products in human tissues. *Lab Invest.* **78(12)**: 1591-1606.

Luo D, Sun H, Xiao RP, and Han Q (2005) Caffeine induced Ca^{2+} release and capacitative Ca^{2+} entry in human embryonic kidney (HEK293) cells. *Eur J Pharmacol* **509(2-3)**: 109-115.

Makita Z, Vlassara H, Rayfield E, Cartwright K, Friedman E, Rodby R, Cerami A, and Bucala R (1992) Hemoglobin-AGE: a circulating marker of advanced glycosylation. *Science* **258(5082)**: 651-3.

Marks AR (2002) Ryanodine receptors, FKBP12, and heart failure *Front Biosci* **1(7)**: d970-d977.

Meissner G (2002) Regulation of mammalian ryanodine receptors. *Front Biosci* **1(7)**: d2072-d2080.

Miyata T, Kurokawa K, and van Ypersele de Strihou C. Relevance of oxidative and carbonyl stress to long-term uremic complications (2000) *Kidney Int Suppl* **76**: S120-S125.

Mitra R, and Morad R (1995) A uniform enzymatic method for dissociation of myocytes from hearts and stomachs of vertebrates. *Am J Physiol* **249(5 Pt 2)**: H1056-H1060.

Nagaraj RH, Oya-Ito T, Padayatti PS, Kumar R, Mehta S, West K, Levison B, Sun J, Crabb JW, and Padival AK (2003) Enhancement of chaperone function of alpha-crystallin by methylglyoxal modification. *Biochemistry* **42(36)**: 10746-10755.

Nagai R, Horiuchi S, and Unno Y (2003) Application of monoclonal antibody libraries for the measurement of glycation adducts. *Biochem Soc Trans* **31(Pt 6)**: 1438-1440.

Nagai R, Fujiwara Y, Mera K, Motomura K, Iwao Y, Tsurushima K, Nagai M, Takeo K, Yoshitomi M, Otagiri M, and Ikeda T (2008) Usefulness of antibodies for evaluating the biological significance of AGEs. *Ann N Y Acad Sci* **1126**: 38-41.

National Research Council (1996) *Guide for the Care and Use of Laboratory Animals*. National Academy Press, Washington, DC.

Nemet I, Varga-Defterdarović L, and Turk Z (2004) Preparation and quantification of methylglyoxal in human plasma using reverse-phase high-performance liquid chromatography. *Clin Biochem* **37(10)**: 875-881.

Netticadan T, Temsah RM, Kent A, Elimban V, and Dhalla NS (2001) Depressed levels of Ca^{2+}-cycling proteins may underlie sarcoplasmic reticulum dysfunction in the diabetic heart. *Diabetes* **50(9)**: 2133-2138.

Oya T, Hattori N, Mizuno Y, Miyata S, Maeda S, Osawa T, and Uchida K (1999) Methylglyoxal modification of protein. Chemical and immunochemical characterization of methylglyoxal-arginine adducts. *J Biol Chem.* **274(26)**: 18492-184502.

Pereira L, Matthes J, Schuster I, Valdivia HH, Herzig S, Richard S, and Gómez AM (2006) Mechanisms of $[Ca^{2+}]_i$ transient decrease in cardiomyopathy of db/db type 2 diabetic mice. *Diabetes* **55(3)**: 608-615.

Priego-Capote F, and Sanchez JC (2009) Strategies for proteomic analysis of non-enzymatically glycated proteins *Mass Spectrom Rev* **28(1)**: 135-146.

Segré CV, and Chiocca S (2011) Regulating the regulators: the post-translational code of class I HDAC1 and HDAC2. *J Biomed Biotechnol* **2011**: 690848-690863.

Shao CH, Capek HL, Patel KP, Wang M, Tang K, DeSouza C, Nagai R, Mayhan W, Periasamy M, and Bidasee KR (2011) Carbonylation contributes to SERCA2a activity loss and diastolic dysfunction in a rat model of type 1 diabetes. *Diabetes* **60(3)**: 947-959.

Shao CH, Rozanski GJ, Nagai R, Stockdale FE, Patel KP, Wang M Singh J, Mayhan WG, and Bidasee KR (2010) Carbonylation of myosin heavy chains in rat heart during diabetes. *Biochem Pharmacol* **80**: 205–217.

Shao CH, Rozanski GJ, Patel KP, and Bidasee KR (2007) Dyssynchronous (non-uniform) Ca^{2+} release in myocytes from streptozotocin-induced diabetic rats. *J Mol Cell Cardiol* **42(1)**: 234-246.

Shao CH, Wehrens XH, Wyatt TA, Parbhu S, Rozanski GJ, Patel KP, and Bidasee KR (2009) Exercise training during diabetes attenuates cardiac ryanodine receptor dysregulation. *J Appl Physiol* **106**: 1280–1292.

Slatter DA, Avery NC, and Bailey AJ (2004) Identification of a new cross-link and unique histidine adduct from bovine serum albumin incubated with malondialdehyde. *J Biol Chem* **279(1)**: 61-69.

Suetomi T, Yano M, Uchinoumi H, Fukuda M, Hino A, Ono M, Xu X, Tateishi H, Okuda S, Doi M, Kobayashi S, Ikeda Y, Yamamoto T, Ikemoto N, and Matsuzaki M (2011) Mutation-Linked Defective Interdomain Interactions Within Ryanodine Receptor Cause Aberrant Ca^{2+} Release Leading to Catecholaminergic Polymorphic Ventricular Tachycardia. *Circulation* **124(6)**: 682-694.

Tian C, Hong Shao C, Moore CJ, Kutty S, Walseth T, Desouza C, and Bidasee KR (2011) Gain of function of cardiac ryanodine receptor in a rat model of type 1 diabetes. *Cardiovasc Res* **91(2)**: 300-309.

Uchida K (2000) Role of reactive aldehyde in cardiovascular diseases. *Free Radic Biol Med* **28(12)**: 1685-1696.

Vander Jagt DL (2008) Methylglyoxal, diabetes mellitus and diabetic complications. *Drug Metabol Drug Interact* **23(1-2)**: 93-124.

Vicentini J, Valentini J, Grotto D, Paniz C, Roehrs M, Brucker N, Charão MF, Moro AM, Tonello R, Moreira AP, Buffon A, Beck M, and Garcia SC (2011) Association among microalbuminuria and oxidative stress biomarkers in patients with type 2 diabetes. *J Investig Med* **59(4)**: 649-654.

Watanabe H, and Knollmann BC (20110 Mechanism underlying catecholaminergic polymorphic ventricular tachycardia and approaches to therapy. *J Electrocardiol* **44(6)**: 650-655.

Williams ME, Bolton WK, Khalifah RG, Degenhardt TP, Schotzinger RJ, and McGill JB (2007) Effects of pyridoxamine in combined phase 2 studies of patients with type 1 and type 2 diabetes and overt nephropathy. *Am J Nephrol.* **27(6)**: 605-614.

Wong CM, Marcocci L, Liu L, and Suzuki YJ (2010) Cell signaling by protein carbonylation and decarbonylation. *Antioxid Redox Signal* **12(3)**: 393-404.

World Health Organization (2011) http://www.who.int/mediacentre/factsheets/fs312/en/ (accessed May 12th, 2012).

Yano M, Yamamoto T, Kobayashi S, and Matsuzaki M (2009) Role of ryanodine receptor as a Ca^{2+} regulatory center in normal and failing hearts. *J Cardiol* **53(1)**: 1-7.

Yaras N, Ugur M, Ozdemir S, Gurdal H, Purali N, Lacampagne A, Vassort G, and Turan B (2005) Effects of diabetes on ryanodine receptor Ca release channel (RyR2) and Ca^{2+} homeostasis in rat heart. *Diabetes* **54**: 3082–3088.

Zhong Y, Ahmed S, Grupp IL, and Matlib MA (2001) Altered SR protein expression associated with contractile dysfunction in diabetic rat hearts. *Am J Physiol Heart Circ Physiol* **281(3)**: H1137-1147.

Zhou L, Aon MA, Liu T, and O'Rourke B (2011) Dynamic modulation of Ca^{2+} sparks by mitochondrial oscillations in isolated guinea pig cardiomyocytes under oxidative stress. *J Mol Cell Cardiol* **51(5)**: 632-639.

Molecular Pharmacology Fast Forward. Published on May 30, 2012 as DOI: 10.1124/mol.112.078352
This article has not been copyedited and formatted. The final version may differ from this version.

FOOTNOTES

Dr. Chun Hong Shao, Dr. Chengju Tian, and Dr. Shouqiang Ouyang contributed equally.

This work was supported in part by grants from the Edna Ittner Research Foundation, American Diabetes Association [1-06-RA-11], National Institutes of Health [HL085061] and Grant-in-Aid from the Ministry of Education, Science, Sports and Cultures of Japan [18790619].

Molecular Pharmacology Fast Forward. Published on May 30, 2012 as DOI: 10.1124/mol.112.078352
This article has not been copyedited and formatted. The final version may differ from this version.

FIGURE LEGENDS

Fig. 1. *Ex vivo* ventricular function. (i) Basal and isoproterenol-induced changes in left ventricular tension in *ex vivo* hearts from control (C), diabetic (D), and insulin-treated diabetic (Ins-D) animals. Values shown are for n ≥ 14 hearts. * Significantly different from control ($p < 0.05$), ** significantly different from diabetic ($p < 0.05$). **(ii)** Representative original tracing of left ventricular response of hearts from control (C), diabetic (D), and insulin-treated diabetic (Ins-D) challenged with 1 and 10 nM isoproterenol. Abnormal ventricular contractions are shown with red arrows.

Fig. 2. Alterations in RyR2 activity in diabetic myocytes. (i) Representative line-scan images of spontaneous Ca^{2+} release (Ca^{2+} sparks) in myocytes from control (C), diabetic (D), and insulin-treated animals (Ins-D). **(ii)** Representative evoked Ca^{2+} transients from control (C), diabetic (D), and insulin-treated diabetic (Ins-D) myocytes with stimulation at 0.5 Hz stimulation. **(ii)** Representative electron microscopic images of dyad junction from control (C), diabetic (D), and insulin-treated animals (Ins-D). SR = sarcoplasmic reticulum, IFM = interfibrillar mitochondrion, T= T-tubule. Scale bar at bottom is 100 nm.

Fig. 3. Posttranslational modification of RyR2 by reactive carbonyl species during diabetes. **(i)** Representative autoradiograms showing steady state level of RyR2 protein in membrane

Molecular Pharmacology Fast Forward. Published on May 30, 2012 as DOI: 10.1124/mol.112.078352
This article has not been copyedited and formatted. The final version may differ from this version.

vesicles isolated from control (C), diabetic (D) and insulin-treated diabetic (Ins-D) rat hearts. Graph below shows normalized [^{3}H]ryanodine binding (mean ± S.E.M, n >4 experiments). **(ii)** Representative autoradiograms showing carbonyl adducts on RyR2 from control (C), diabetic (D) and insulin-treated diabetic (Ins-D) rat hearts. Immunoblots were obtained employing 60 µg of membrane vesicles employing N^{ε}-carboxy(methyl)lysine (CML), argpyrimidine, AGEs, 3-deoxyglycosone/hydroimidazolone, GA-pyridine, pentosidine, and pyrraline as the primary antibodies in Western blot assays (1:1000 for 16 hrs). **(iii)** Relative levels (mean ± S.E.M) of carbonyl adducts on RyR2 in hearts from control (C), diabetic (D) and insulin-treated diabetic (Ins-D) animals. Values shown are from four separate preparations. * Significantly different from control, # significantly different from diabetic ($p < 0.05$). **(iv)** Alignment of MALDI-TOF mass spectra obtained following trypsin digestion of RyR2 from control (C), diabetic (D) and insulin-treated diabetic (Ins-D) rats. M+1 peak is present at 1202.60 Da in diabetic samples but not in the other samples. Perl algorithm predicts this peak is imidazolone B on R4462 ($_{4461}$L**R**QLTHTHR$_{4469}$). **(v)** Y and b ions obtained following fragmentation of 1202.60 Da M+1 mass peak. **(vi)** Red filled circles show locations of carbonyl adducts on RyR2. Black filled circles show the position of other amino acids for reference. The structure of RyR2 has been adapted on a structure published by Jóna and Nánási *Cardiovasc Res*. 2006;**71(3)**: 416-418.

Fig. 4. Mutations to mimic carbonylation alter Ca^{2+}-depending binding of [^{3}H]ryanodine to RyR2. Equal amounts of RyR2 protein were used for this study (inset). Panel **(i)** shows R1611 mutants, panel **(ii)** shows wild type and K2190 mutants, panel **(iii)** shows wild type and K2887

Molecular Pharmacology Fast Forward. Published on May 30, 2012 as DOI: 10.1124/mol.112.078352
This article has not been copyedited and formatted. The final version may differ from this version.

mutants, panel **(iv)** shows wild type and R1611, K2190 and K2887 double mutants, panel **(v)** shows wild type and R4462 mutants, and panel **(vi)** shows wild type and R4682 mutants. Data for each panel represent means ± S.E.M from four experiments. *Significantly different from wild type RyR2 ($p < 0.05$).

Fig. 5. Mutations to mimic carbonylation alter cytoplasmic Ca^{2+} responsiveness of RyR2. (i) Representative 1 sec single channel responses of wild type and RyR2 mutants to increasing *cis* Ca^{2+}. **(ii)** Mean open probability for ≥9 channels for each mutant. S.E.Ms were between 4-8% and left out for clarity. **(iii)** Mean conductance of wild type and RyR2 mutants. * Significantly different ($p < 0.05$) from wild type RyR2.

Fig. 6. Carbonylation-mimicking mutations alter cellular Ca^{2+} responsiveness of RyR2. (i) Representative intracellular Ca^{2+} cycling traces of HEK-293T cells transfected with K2888W, R4462Y and wild type RyR2 subjected to increasing concentration of media Ca^{2+}. Black arrow indicates start of caffeine challenge which continues for 300 sec. **(ii)** Mean number of cells exhibiting intracellular Ca^{2+} oscillation as a function of media Ca^{2+} (n = 5 for >30 cells per mutant). *Significantly different ($p < 0.05$) from wild type RyR2.

Molecular Pharmacology Fast Forward. Published on May 30, 2012 as DOI: 10.1124/mol.112.078352
This article has not been copyedited and formatted. The final version may differ from this version.

Fig. 7. Methylglyoxal (MGO) alters activity of RyR2. (i) The ability of MGO to displace [^{3}H]ryanodine from RyR2. Data shown is the average of six experiments conducted using three separate membrane preparations. **(ii)** Effect of pre-incubating SR membrane vesicles with varying amounts of MGO on Ca^{2+}-dependent binding of [^{3}H]ryanodine to RyR2. Data shown is the average of six experiments done using three separate membrane preparations **(iii)** Representative 1 sec single channel responses of cRyR2 to increasing *cis* concentration of MGO at +35 mV holding potential. **(iv)** Mean open probability ± S.E.M of cRyR2 to increasing [MGO] at 35 mV holding potential, with 3.3 μM cis Ca^{2+} and 250 mM symmetric KCl (n ≥10 channels). **(v)** Mean conductance ± S.E.M of RyR2 to increasing [MGO] at 35 mV holding potential, with 3.3 μM cis Ca^{2+} and 250 mM symmetric KCl (n ≥10 channels). * Significantly different ($p < 0.05$) from wild type RyR2.

Fig. 8. **Methylglyoxal (MGO) alters intracellular Ca^{2+} homeostasis in healthy myocytes. (i)** Time-lapsed confocal images showing changes in intracellular Ca^{2+} release in a myocyte acutely exposed to 20 μM MGO and monitored for >6 minutes. Red arrows indicate spontaneous Ca^{2+} releases. White arrows show elevation in nuclear Ca^{2+}. Experiments were conducted in 18 cells from 4 separate myocytes preparations, all of which exhibited behavior similar when challenged with MGO. **(ii)** Representative line scanned images of spontaneous and evoked Ca^{2+} releases in myocytes acutely exposed to 20 μM MGO and monitored for >6 minutes. Black arrows show stimulation at 0.25 Hz. White arrows show spontaneous Ca^{2+} release, green arrows show sites of

Molecular Pharmacology Fast Forward. Published on May 30, 2012 as DOI: 10.1124/mol.112.078352
This article has not been copyedited and formatted. The final version may differ from this version.

non-uniform evoked Ca^{2+} release. Experiments were conducted in 22 cells from 4 separate myocyte preparations, 18 exhibited characteristics similar to that shown above.

Fig. 9: Methylglyoxal increases mitochondrial superoxide production. Time-lapsed confocal images showing production of superoxide (red images, **(i)**), and total ROS (red images, **iv**) in a myocyte following exposure to 20 μM MGO. Green images in **(ii)** and **(v)** represent MitoTracker® Green (mitochondria) and red images in **(ii)** and **(iv)** represent MitoSox® signal monitored by 404 nm excitation or 488 nm excitation, respectively. Green-red overlay images showing superoxide and ROS in mitochondria are shown in right panel of **(ii)** and **(iv)**. Mean ± S.E.M production of superoxide and ROS produced in mitochondria before and after 15 and 16 minutes, respectively are shown in **(iii)** and **(vi)**. * Significantly different from before ($p < 0.05$).

Fig. 10. Treatment of diabetic rats with scavengers of reactive carbonyl species blunts RyR2 dysregulation. (i) Representative evoked Ca^{2+} transients in ventricular myocytes isolated from control (C), diabetic (D), Py-treated control (Py-C), Py-treated diabetic (Py-D), Ag-treated control (Ag-C) and AG-treated diabetic (Ag-D) rats**.** Myocytes were stimulated at 1 Hz (black arrow). Experiments were conducted in ≥30 cells from 4 separate myocyte preparations per experimental group. (**ii)** Representative autoradiograms of carbonyl adducts in ventricular heart homogenates from D, Py-C, Py-D, Ag-C and Ag-D rats. Experiments were conducted with four separate JSRV preparations and mean ± S.E.M are shown in panel **(iii)**. * Significantly different from control ($p < 0.05$), # significantly different from diabetic ($p < 0.05$). Panel **(iv)** shows a

Molecular Pharmacology Fast Forward. Published on May 30, 2012 as DOI: 10.1124/mol.112.078352
This article has not been copyedited and formatted. The final version may differ from this version.

representative autoradiograms of steady state level of RyR2 and β-actin proteins in membrane vesicles isolated isolated hearts of control (C), diabetic (D), Py-treated control (Py-C), Py-treated diabetic (Py-D), Ag-treated control (Ag-C) and AG-treated diabetic rats. Graph below shows the ability of equivalent amounts of RyR2 protein from control (C), diabetic (D), Py-treated control (Py-C), Py-treated diabetic (Py-D), Ag-treated control (Ag-C) and AG-treated diabetic hearts to bind [^{3}H]ryanodine. Experiments were conducted ≥ 5 times using 4 different membrane preparations. * Significantly different from control ($p < 0.05$), # significantly different from diabetic ($p < 0.05$). Panel **(v)** shows representative caffeine-induced Ca^{2+} transients in ventricular myocytes isolated from control (C), diabetic (D), Py-treated control (Py-C), Py-treated diabetic (Py-D), Ag-treated control (Ag-C) and AG-treated diabetic hearts. First three black arrows indicate electrically evoked stimulation; last black arrow (right side) indicates application of caffeine. Experiments were done 5 times.

Molecular Pharmacology Fast Forward. Published on May 30, 2012 as DOI: 10.1124/mol.112.078352
This article has not been copyedited and formatted. The final version may differ from this version.

Table 1: General characteristics of animals used in the study

PARAMETER	**Control**	**STZ-diabetic**	**Insulin-treated diabetic**	**Pyridoxamine-treated control**	**Pyridoxamine-treated diabetic**	**Aminoguanidine-treated control**	**Aminoguanidine-treated diabetic**
	(C)	**(D)**	**(Ins-D)**	**(Py-C)**	**(Py-D)**	**(Ag-C)**	**(Ag-D)**
	n = 48	**n = 48**	**n = 48**	**n = 14**	**n = 15**	**n = 15**	**n = 15**
Body mass (g)	370.0 ± 13.3	290.1 ± 17.3*	324.0 ± 7.5	397.6 ± 12.9	283.5 ± 12.6	403.3 ± 7.8	304 ± 10.1
Blood glucose (mmol)	5.0 ± 0.5	21.1 ± 1.4*	8.1 ± 2.1	4.9 ± 1.1	20.1 ± 1.6	8.10 ± 0.33	22.02 ± 2.12
Heart rate (beats per min)	370.2 ± 10.2	283.9 ± 13.2*	327.5 ± 7.5	307 ± 20.6	282.1 ± 29.0	417.0 ± 19.8	294.1 ± 30.2
% Fractional shortening	60.9 ± 3.2	49.3 ± 1.0*	56.3 ± 2.6	58.9 ± 3.1	57.4 ± 3.7**	57.9 ± 1.9	56.4 ± 3.7**
% Ejection fraction	83.5 ± 2.2	72.5 ± 1.0*	80.3 ± 3.5**	84.4 ± 5.2	81.5 ± 3.9**	81.8 ± 2.9	80.1 ±. 3.5**
% Glycosylated hemoglobin	4.1 ± 0.1	7.2 ± 0.1*	4.7 ± 0.2	4.2 ± 0.2	7.6 ± 0.3	4.23 ± 0.21	8.2 ± 0.17
Serum insulin (ng/ml)	1.02 ± 0.21	0.31 ± 0.03*	0.91 ± 0.02	1.10 ± 0.07	0.28 ± 0.04	0.67 ± 0.07	0.31 ± 0.03
Serum TBARS (nmol/ml)	2.4 ± 0.3	11.1 ± 1.9*	4.1 ± 1.0	1.0 ± 0.2	8.0 ± 0.9	4.1 ± 0.9	7.2 ± 0.7**
Serum SSAO activity (units/ml/min)	0.32 ± 0.02	0.56 ± 0.03*	0.35 ± 0.06**	0.22 ± 0.01	0.39 ± 0.02**	0.47 ± 0.03*	0.41 ± 0.05**
Ventricular MGO (µM/100 mg tissue)	1.8 ± 0.2 (n = 6)	4.2 ± 0.6* (n = 6)	2.2 ± 0.4** (n = 6)	ND	ND	ND	ND

* = significantly different from control ($p < 0.05$), ** = significantly different from diabetic ($p < 0.05$), ND = not done

(i)

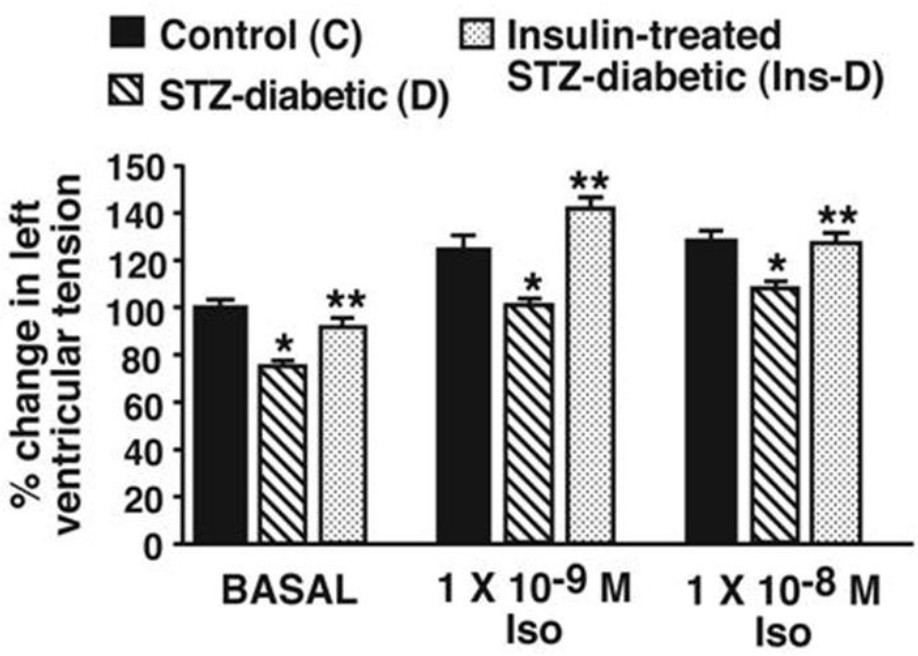
Control (C)
Insulin-treated STZ-diabetic (Ins-D)
STZ-diabetic (D)
% change in left ventricular tension
150
140
120
100
80
60
40
20
0
*
**
BASAL
1 X 10-9 M Iso
1 X 10-8 M Iso

(ii)

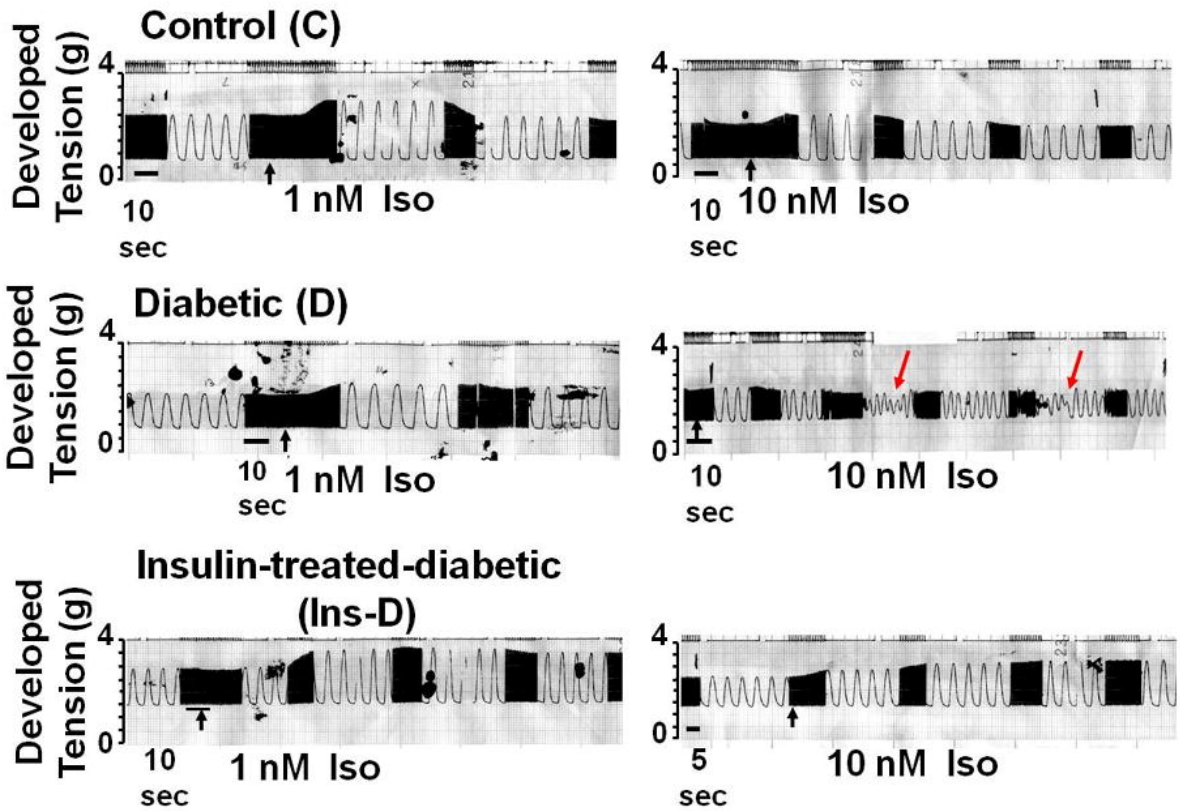
Control (C)
Developed Tension (g)
4
0
10 sec
1 nM Iso
10 nM Iso
Diabetic (D)
Insulin-treated-diabetic (Ins-D)
5 sec

Figure 1

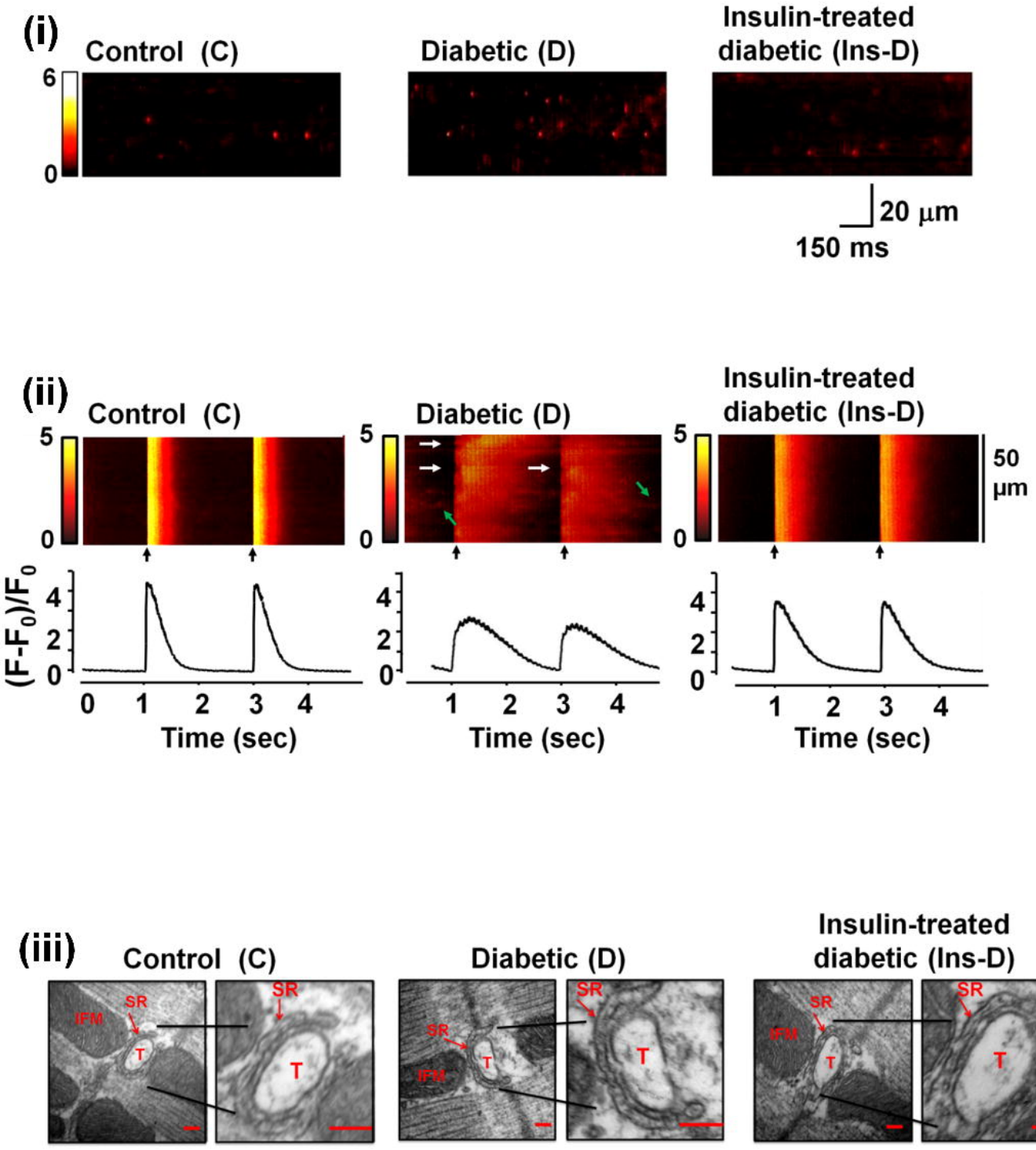
(i)
Control (C)
Diabetic (D)
Insulin-treated diabetic (Ins-D)
6
0
20 μm
150 ms
(ii)
Control (C)
Diabetic (D)
Insulin-treated diabetic (Ins-D)
5
0
50 μm
(F-F0)/F0
4
2
0
0 1 2 3 4
Time (sec)
(iii)
Control (C)
Diabetic (D)
Insulin-treated diabetic (Ins-D)
SR
IFM
T

Figure 2

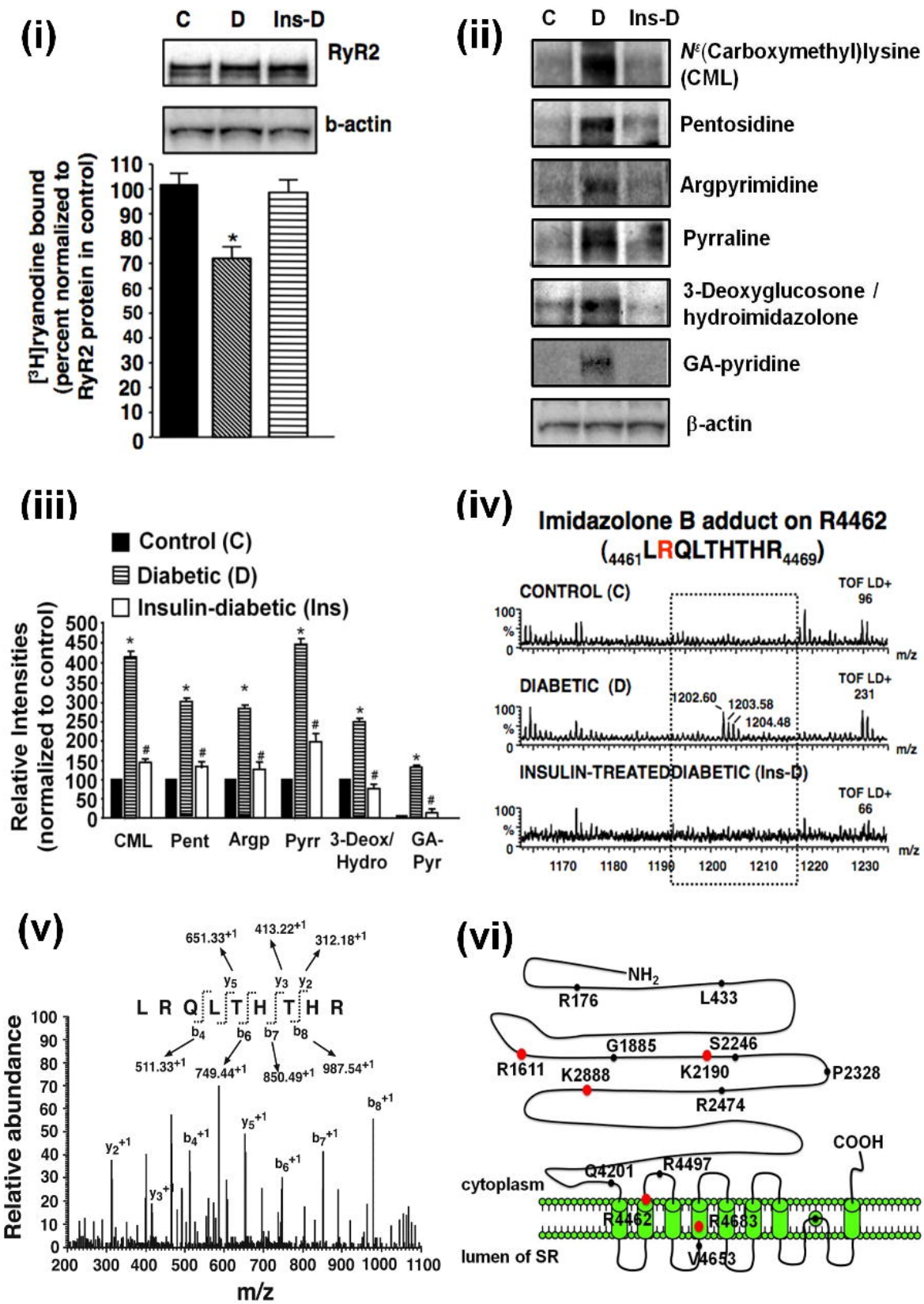
(i)
C
D
Ins-D
RyR2
b-actin
[3H]ryanodine bound (percent normalized to RyR2 protein in control)
(ii)
Nε(Carboxymethyl)lysine (CML)
Pentosidine
Argpyrimidine
Pyrraline
3-Deoxyglucosone / hydroimidazolone
GA-pyridine
β-actin
(iii)
Control (C)
Diabetic (D)
Insulin-diabetic (Ins)
Relative Intensities (normalized to control)
CML
Pent
Argp
Pyrr
3-Deox/ Hydro
GA-Pyr
(iv)
Imidazolone B adduct on R4462
(4461LRQLTHTHR4469)
CONTROL (C)
DIABETIC (D)
INSULIN-TREATED DIABETIC (Ins-D)
TOF LD+
1202.60
1203.58
1204.48
m/z
(v)
L R Q L T H T H R
Relative abundance
m/z
(vi)
NH2
R176
L433
G1885
S2246
R1611
K2888
K2190
P2328
R2474
COOH
Q4201
R4497
cytoplasm
R4462
R4683
lumen of SR
V4653

Figure 3

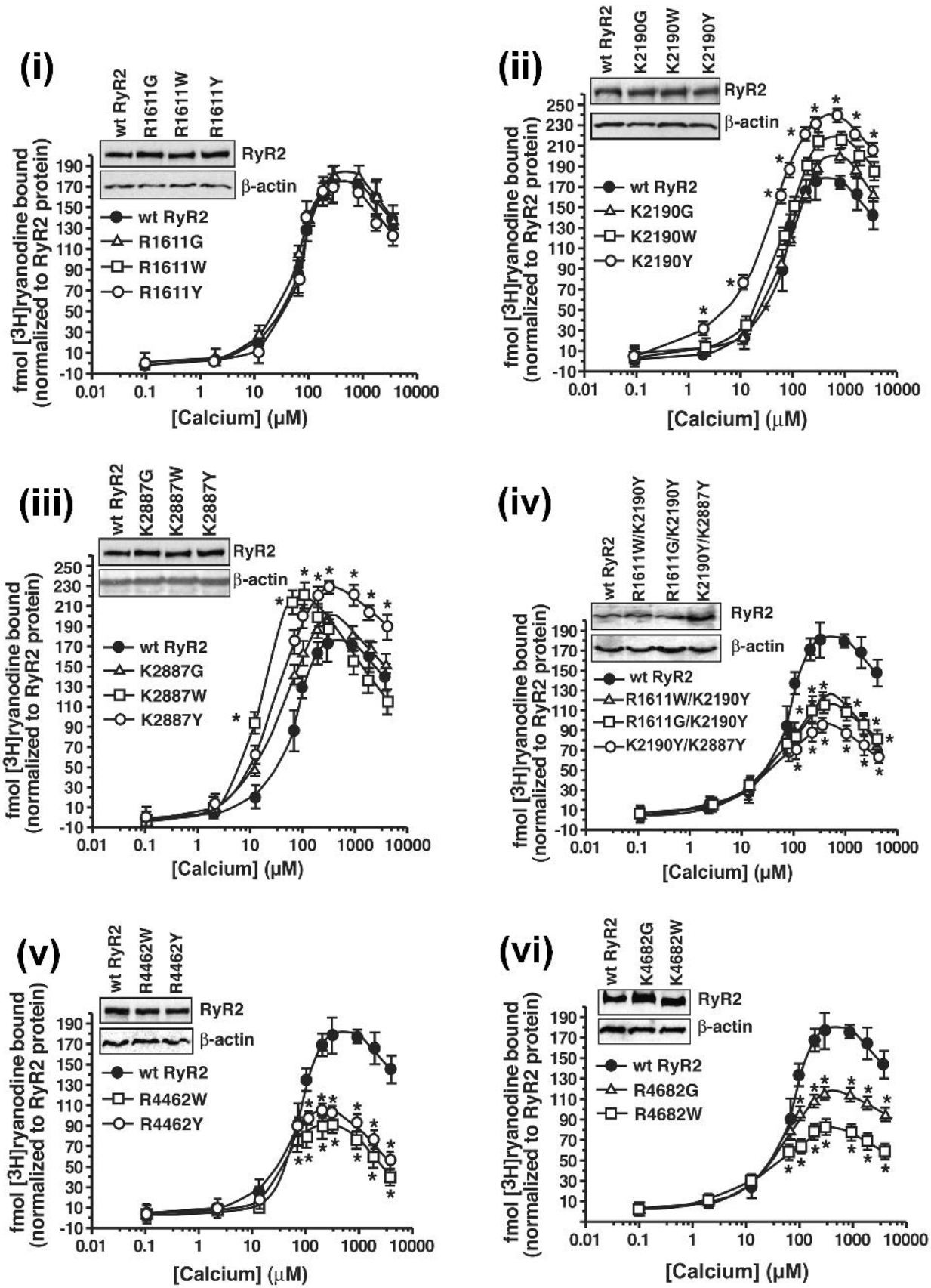
(i)
wt RyR2
R1611G
R1611W
R1611Y
RyR2
β-actin
wt RyR2
R1611G
R1611W
R1611Y
fmol [3H]ryanodine bound (normalized to RyR2 protein)
[Calcium] (μM)
(ii)
wt RyR2
K2190G
K2190W
K2190Y
RyR2
β-actin
wt RyR2
K2190G
K2190W
K2190Y
fmol [3H]ryanodine bound (normalized to RyR2 protein)
[Calcium] (μM)
(iii)
wt RyR2
K2887G
K2887W
K2887Y
RyR2
β-actin
wt RyR2
K2887G
K2887W
K2887Y
fmol [3H]ryanodine bound (normalized to RyR2 protein)
[Calcium] (μM)
(iv)
wt RyR2
R1611W/K2190Y
R1611G/K2190Y
K2190Y/K2887Y
RyR2
β-actin
wt RyR2
R1611W/K2190Y
R1611G/K2190Y
K2190Y/K2887Y
fmol [3H]ryanodine bound (normalized to RyR2 protein)
[Calcium] (μM)
(v)
wt RyR2
R4462W
R4462Y
RyR2
β-actin
wt RyR2
R4462W
R4462Y
fmol [3H]ryanodine bound (normalized to RyR2 protein)
[Calcium] (μM)
(vi)
wt RyR2
K4682G
K4682W
RyR2
β-actin
wt RyR2
R4682G
R4682W
fmol [3H]ryanodine bound (normalized to RyR2 protein)
[Calcium] (μM)

Figure 4

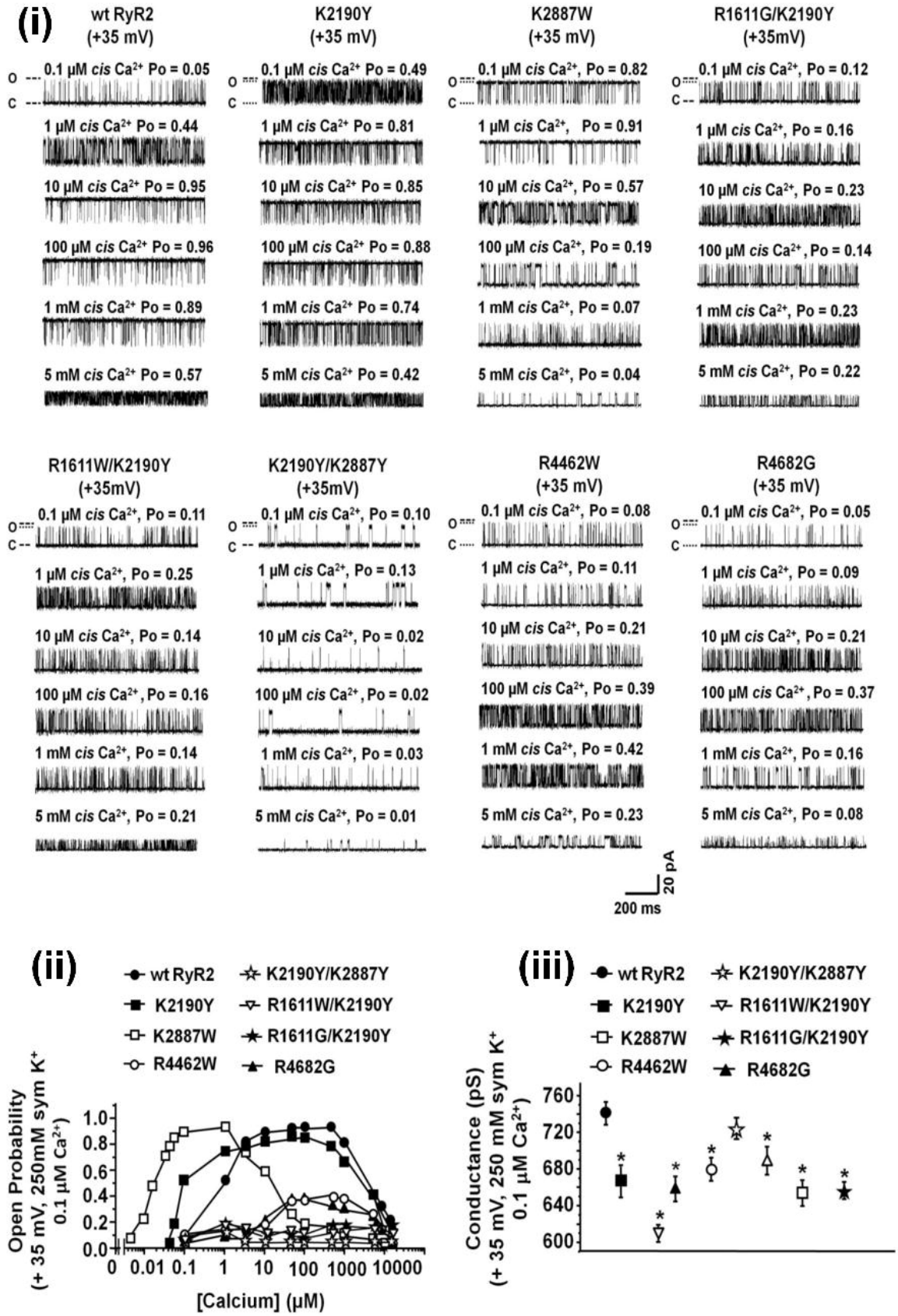
(i)
wt RyR2 (+35 mV)
K2190Y (+35 mV)
K2887W (+35 mV)
R1611G/K2190Y (+35mV)
R1611W/K2190Y (+35mV)
K2190Y/K2887Y (+35mV)
R4462W (+35 mV)
R4682G (+35 mV)
O
C
20 pA
200 ms
(ii)
wt RyR2
K2190Y
K2887W
R4462W
K2190Y/K2887Y
R1611W/K2190Y
R1611G/K2190Y
R4682G
Open Probability (+ 35 mV, 250mM sym K+ 0.1 µM Ca2+)
[Calcium] (µM)
(iii)
Conductance (pS) (+ 35 mV, 250 mM sym K+ 0.1 µM Ca2+)

Figure 5

(i)

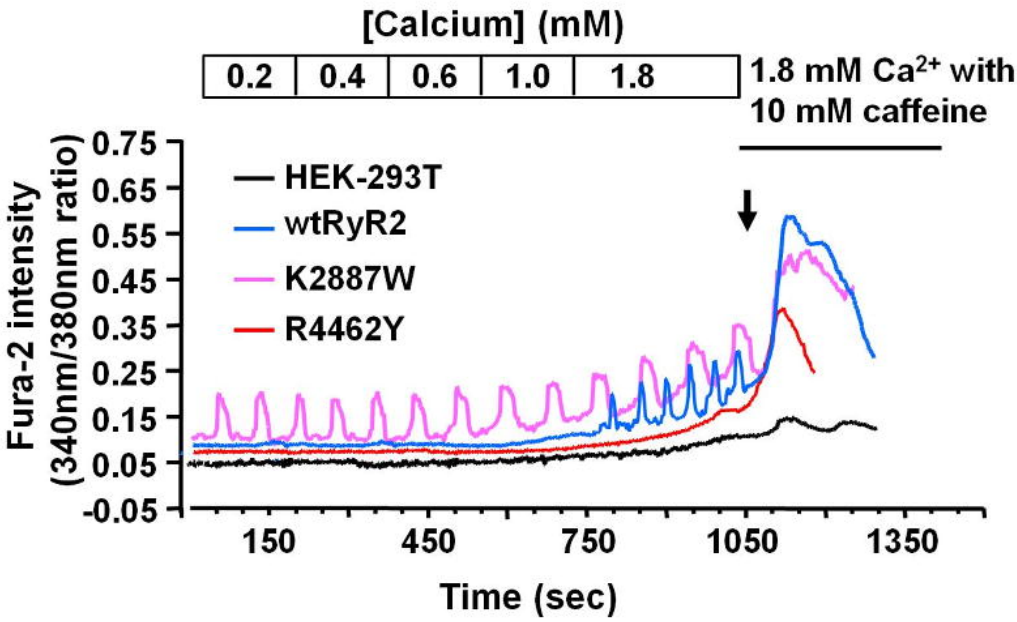
[Calcium] (mM)
0.2
0.4
0.6
1.0
1.8
1.8 mM Ca2+ with
10 mM caffeine
HEK-293T
wtRyR2
K2887W
R4462Y
Fura-2 intensity
(340nm/380nm ratio)
0.75
0.65
0.55
0.45
0.35
0.25
0.15
0.05
-0.05
150
450
750
1050
1350
Time (sec)

(ii)

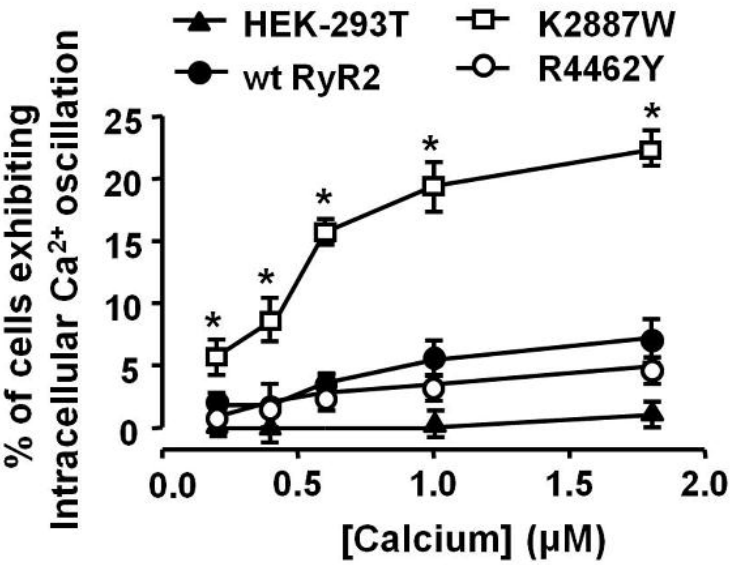
HEK-293T
wt RyR2
K2887W
R4462Y
% of cells exhibiting
Intracellular Ca2+ oscillation
25
20
15
10
5
0
*
0.0
0.5
1.0
1.5
2.0
[Calcium] (μM)

Figure 6

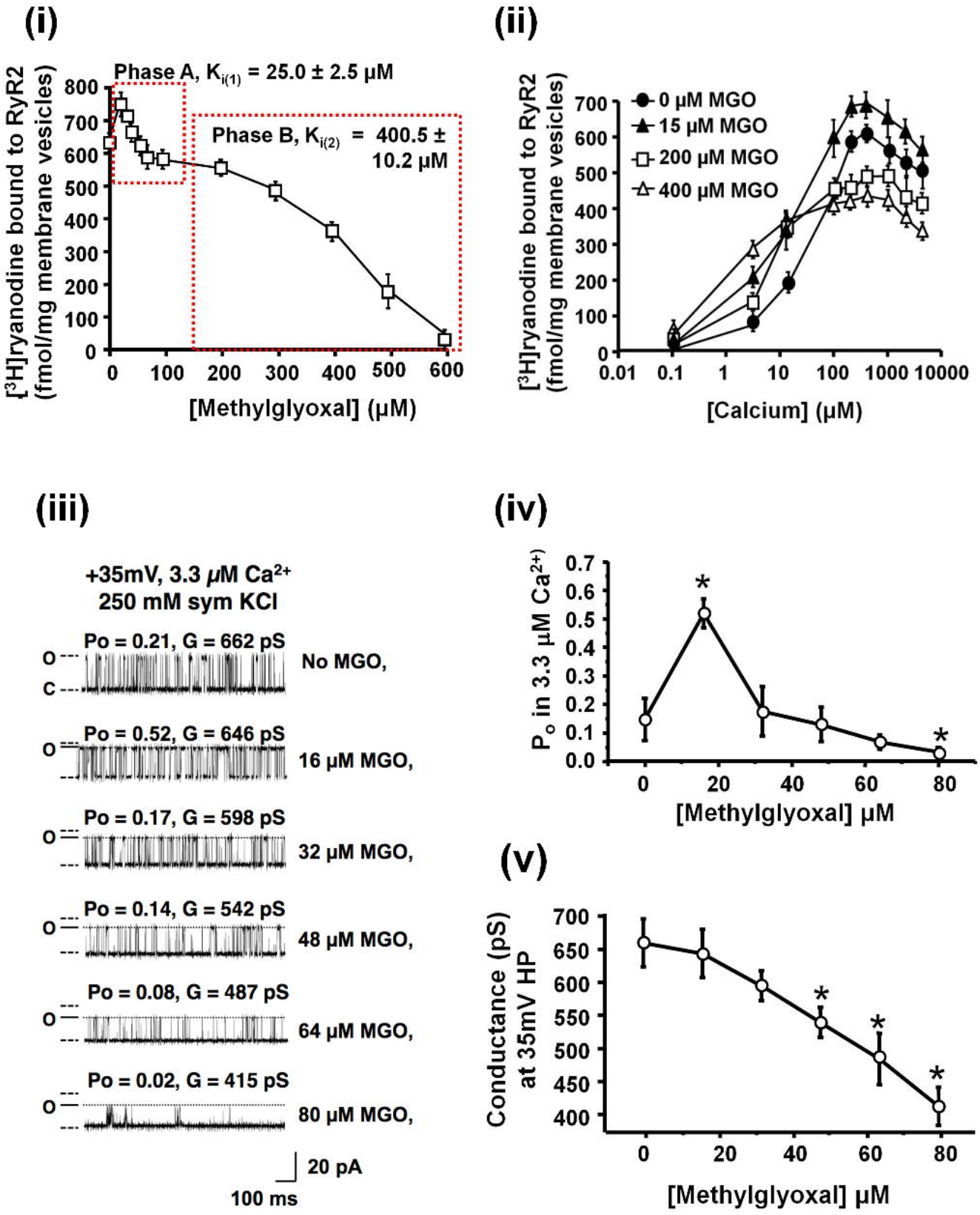
(i)
Phase A, $K_{i(1)}$ = 25.0 ± 2.5 μM
Phase B, $K_{i(2)}$ = 400.5 ± 10.2 μM
[^{3}H]ryanodine bound to RyR2 (fmol/mg membrane vesicles)
[Methylglyoxal] (μM)
(ii)
0 μM MGO
15 μM MGO
200 μM MGO
400 μM MGO
[^{3}H]ryanodine bound to RyR2 (fmol/mg membrane vesicles)
[Calcium] (μM)
(iii)
+35mV, 3.3 μM Ca^{2+}
250 mM sym KCl
Po = 0.21, G = 662 pS
No MGO,
Po = 0.52, G = 646 pS
16 μM MGO,
Po = 0.17, G = 598 pS
32 μM MGO,
Po = 0.14, G = 542 pS
48 μM MGO,
Po = 0.08, G = 487 pS
64 μM MGO,
Po = 0.02, G = 415 pS
80 μM MGO,
20 pA
100 ms
(iv)
P_o in 3.3 μM Ca^{2+}
[Methylglyoxal] μM
(v)
Conductance (pS) at 35mV HP
[Methylglyoxal] μM

Figure 7

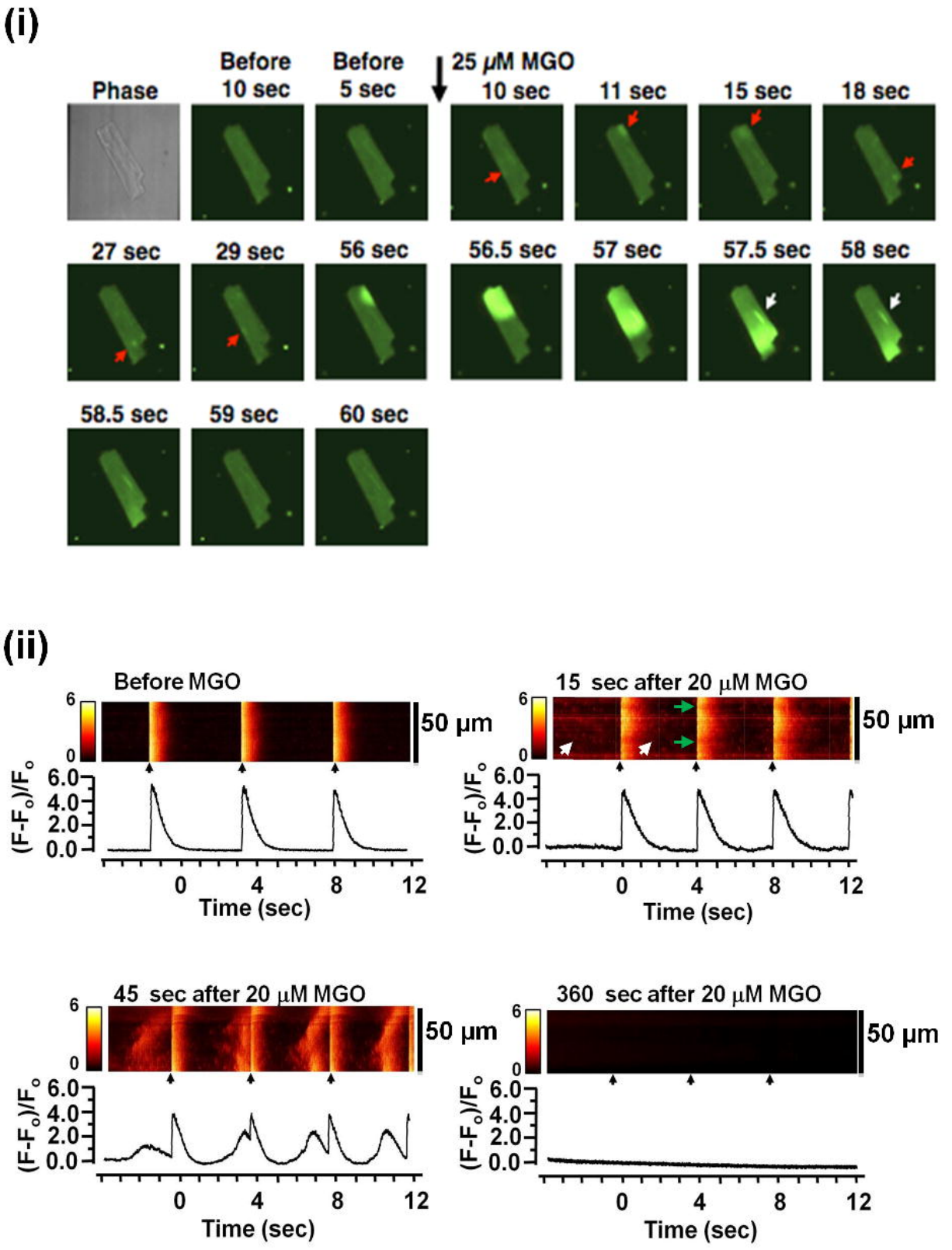
(i)
Phase
Before 10 sec
Before 5 sec
25 μM MGO
10 sec
11 sec
15 sec
18 sec
27 sec
29 sec
56 sec
56.5 sec
57 sec
57.5 sec
58 sec
58.5 sec
59 sec
60 sec
(ii)
Before MGO
15 sec after 20 μM MGO
45 sec after 20 μM MGO
360 sec after 20 μM MGO
50 μm
(F-F0)/F0
Time (sec)

Figure 8

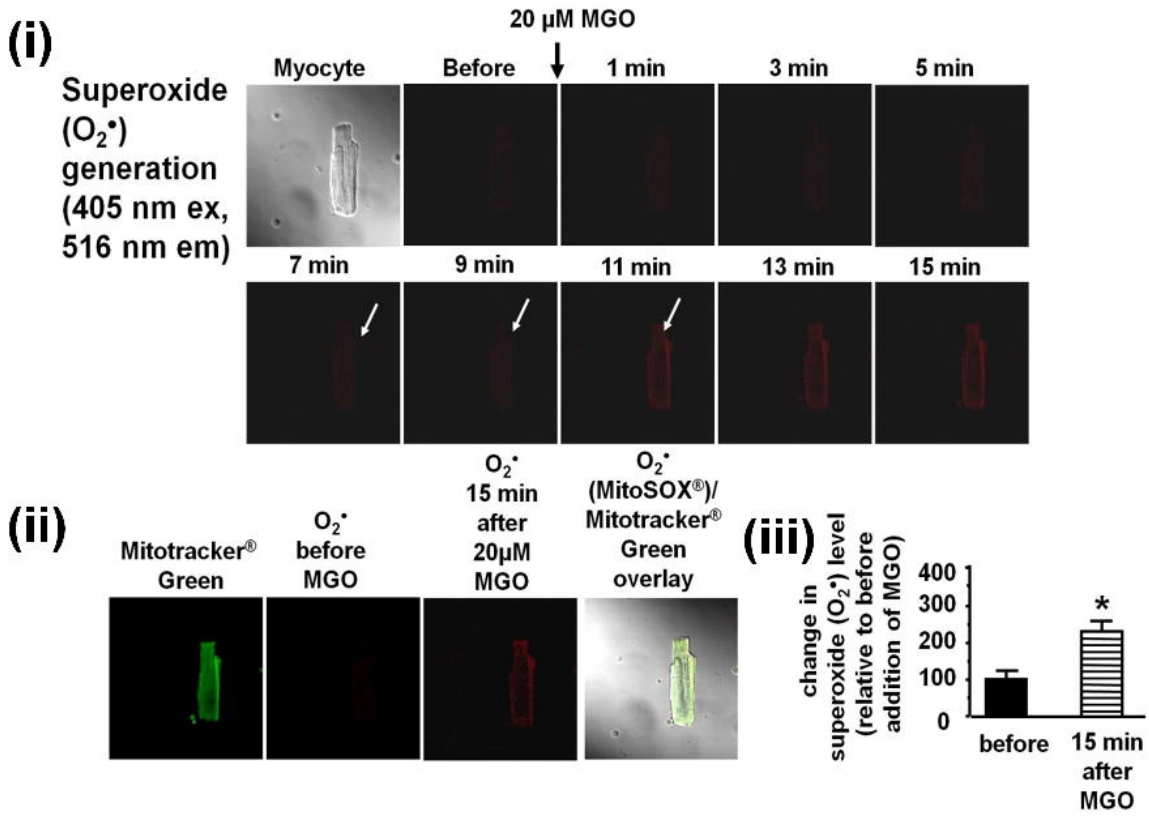
(i)
Superoxide ($O_2^{\bullet}$) generation (405 nm ex, 516 nm em)
20 μM MGO
Myocyte
Before
1 min
3 min
5 min
7 min
9 min
11 min
13 min
15 min
(ii)
Mitotracker® Green
$O_2^{\bullet}$ before MGO
$O_2^{\bullet}$ 15 min after 20μM MGO
$O_2^{\bullet}$ (MitoSOX®)/ Mitotracker® Green overlay
(iii)
change in superoxide ($O_2^{\bullet}$) level (relative to before addition of MGO)
400
300
200
100
0
*
before
15 min after MGO
(iv)
Total ROS generation (488 nm ex, 516 nm em)
20 μM MGO
Myocyte
Before
2 min
4 min
6 min
8 min
10 min
12 min
14 min
16 min
(v)
Mitotracker® Green
Total ROS before MGO
Total ROS 16 min after 20μM MGO
Total ROS (MitoSOX®)/ Mitotracker® Green overlay
(vi)
Percent change in total ROS level (relative to before addition of MGO)
800
600
400
200
0
*
before
16 min after MGO

Figure 9

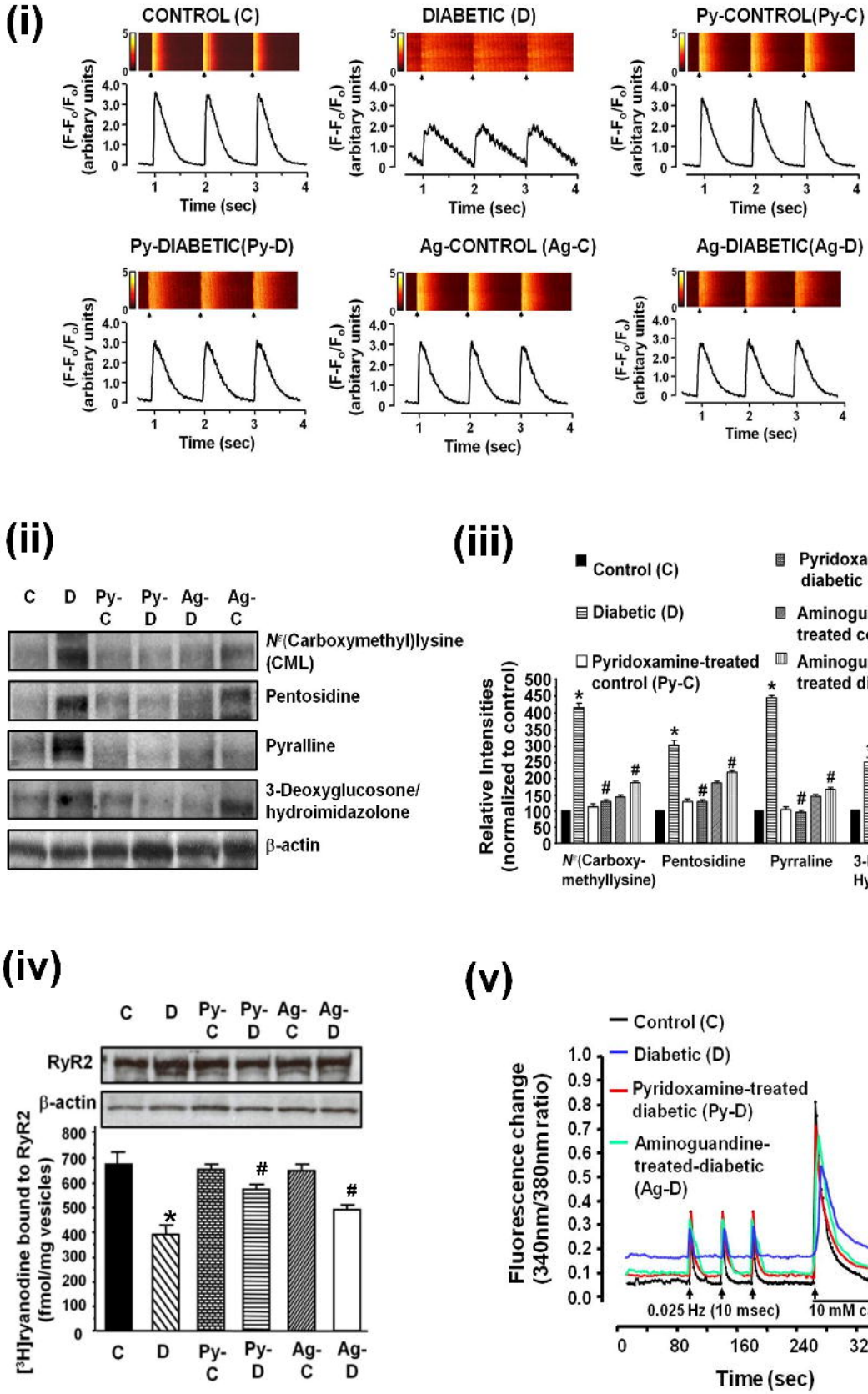
(i)
CONTROL (C)
DIABETIC (D)
Py-CONTROL(Py-C)
Py-DIABETIC(Py-D)
Ag-CONTROL (Ag-C)
Ag-DIABETIC(Ag-D)
(F-Fo/Fo) (arbitary units)
Time (sec)
(ii)
C
D
Py-C
Py-D
Ag-D
Ag-C
Nε(Carboxymethyl)lysine (CML)
Pentosidine
Pyralline
3-Deoxyglucosone/ hydroimidazolone
β-actin
(iii)
Control (C)
Diabetic (D)
Pyridoxamine-treated control (Py-C)
Pyridoxamine-treated diabetic (Py-D)
Aminoguanidine-treated control (Ag-C)
Aminoguanidine-treated diabetic(Ag-D)
Relative Intensities (normalized to control)
Nε(Carboxy-methyllysine)
Pentosidine
Pyrraline
3-Deoxglucosone/ Hydroimidazolone
(iv)
RyR2
β-actin
[3H]ryanodine bound to RyR2 (fmol/mg vesicles)
(v)
Control (C)
Diabetic (D)
Pyridoxamine-treated diabetic (Py-D)
Aminoguandine-treated-diabetic (Ag-D)
Fluorescence change (340nm/380nm ratio)
0.025 Hz (10 msec)
10 mM caffeine
Time (sec)

Figure 10